Fully coupled finite strain consolidation analysis for soft clay treated by prefabricated horizontal drain with vacuum and heat preloading

Yang Liu[1#], An Li[2#], Peichen Wu[3*], Penglin Li[4], Jian-Hua Yin[5], Jun-Jie Zheng[6]

[1] Postdoctoral Fellow, Department of Civil and Environmental Engineering, The Hong Kong Polytechnic University, Hong Kong 999077, China

Email: yang205.liu@polyu.edu.hk; ORCID: https://orcid.org/0000-0003-0990-4084

[2] Ph.D. Candidate, Department of Civil and Environmental Engineering, The Hong Kong Polytechnic University, Hong Kong 999077, China

Email: 21071413r@connect.polyu.hk; ORCID: https://orcid.org/0009-0006-7821-0958

[3] Research Assistant Professor, Department of Civil and Environmental Engineering, The Hong Kong Polytechnic University, Hong Kong 999077, China (Corresponding author)

Email: peicwu@polyu.edu.hk; ORCID: https://orcid.org/0000-0001-7900-3703

[4] Ph.D. Candidate, Department of Civil and Environmental Engineering, The Hong Kong Polytechnic University, Hong Kong 999077, China

Email: pengl.li@connect.polyu.hk; ORCID: https://orcid.org/0000-0003-4440-8457

[5] Chair Professor, Department of Civil and Environmental Engineering, Research Institute of Land and Space, The Hong Kong Polytechnic University, Hong Kong 999077, China

Email: cejhyin@polyu.edu.hk; ORCID: https://orcid.org/0000-0002-7200-3695

[6] Professor, School of Civil Engineering, Wuhan University, Wuhan 430074, China

Email: zhengjunjie@whu.edu.cn; ORCID: https://orcid.org/0000-0001-9679-4914

The authors contribute equally to this paper

Abstract: This paper established a one-dimensional fully coupled finite strain consolidation analysis for soft clay treated by thermal prefabricated horizontal drain under vacuum and heat preloading with the consideration of thermal elastic viscoplastic (TEVP) behaviours of soft clay. First, the governing equations for finite strain consolidation, heat conduction, and heat convention process have been carefully derived based on the well-established Gibson's finite strain consolidation theory and one-dimensional TEVP constitutive model. Secondly, the accuracy and reliability of the numerical method and good performance have been verified with a benchmark case and three physical model tests. Then, the improvement of consolidation efficiency rate (IER) was defined and used to study the effect of three variables on consolidation efficiency. Last but not least, a graphical user interface (GUI) was provided to support researchers and engineers in utilizing the proposed numerical method for conducting consolidation analysis of soft soil treated in the same or similar fashion.

Keywords: Soft soil, finite strain consolidation, prefabricated horizontal drain, vacuum, heating

1. Introduction

Terzaghi (1943) pioneered the notion of the one-dimensional saturated soil consolidation model, which has subsequently spurred significant advancements in research on soil consolidation within the geotechnical engineering field. Several advancements have been achieved in challenging the fundamental assumptions of Terzaghi's consolidation theory (Terzaghi 1923, 1943), leading to the development of several theories or models, including finite strain consolidation (Fox and Berles 1997; Liu et al. 2022b; Pu et al. 2020), electro-osmotic consolidation (Zhao et al. 2020), unsaturated soil consolidation models (Fredlund and Hasan 1979), etc. Among them, research on finite strain consolidation has garnered significant attention and interest in recent decades.

As stated by Vrakas and Anagnostou (2015), when the strain of soil exceeds 10%, the small strain theory is not appropriate for describing the consolidation behaviour of soft soil, especially for the ultra-soft dredged sludge (Chen et al. 2024). Finite strain theory is particularly suitable when the soil possesses a significant initial water content that exceeds the liquid limit, typically leading to a large settlement. In the study of finite strain consolidation, the method of using vacuum pressure and surcharge preloading combined with prefabricated vertical drains (PVDs) was employed to study finite strain consolidation of soft soil (Geng and Yu 2017). Vertical drains, despite their usefulness, have various limits including substantial flexing and loss of vacuum with depth. Chiba et al. (1992) suggested using prefabricated horizontal drains (PHD) for vacuum

71 preloading as a means to address these limitations. The efficiency of the method has
72 been then confirmed by model experiments (Chu et al. 2011; Guo et al. 2013). Most
73 recently, Zhang et al. (2023a) presented a novel method of dewatering dredged sludge
74 using geotextile tubes combined with vacuum-assisted PHDs. The advantages of the
75 method have been shown through experimental and theoretical investigations (Zhang
76 et al. 2023b; Zhang et al. 2022).

77 In addition to vacuum-assisted PVDs or PHDs that can improve the consolidation
78 rate, heating soil can also enhance the consolidation efficiency. Biot (1956) gave a
79 thermal-fluid-structure coupling equations. Britto et al. (1989) introduced a finite
80 element model to examine the heat transfer consolidation issue in a saturated elastic
81 soil with fine-grained particles. Abuel-Naga et al. (2006) investigated the impact of
82 increasing the temperature of soft Bangkok clay on the performance of the preloading
83 process using the PVD. Saowapakpiboon et al. (2009) presented the effects of vacuum
84 and heat preloading of a PVD that was used to accelerate the consolidation of soft
85 Bangkok clay. Artidteang et al. (2011) focused on enhancing the efficiency of
86 consolidation in improving soft Bangkok clay using vacuum and heat preloading.
87 Saowapakpiboon et al. (2011) compared the consolidation efficiency of PVD
88 preloading with and without vacuum and heat to accelerate the consolidation of soft
89 Bangkok clay. Cheng et al. (2017) proposed a semi-analytical method to study the
90 thermal consolidation problem. According to Wang et al. (2020), vacuum preloading
91 can expedite the consolidation rate of soil when it is subjected to a suitable temperature.

Du et al. (2021) employed heating preloading to overcome smear effects induced by the installation of PVD and improve consolidation efficiency. Chen et al. (2023b) found that the treatment combining heating PVD with vacuum preloading can efficiently increase the final settlement of soft soil through physical model tests and molecular dynamics studies. All these studies support that heating the soil is a good way to improve consolidation efficiency.

Considering the limitations of using PVD and the advantages of heat preloading, the method of using vacuum-assisted PHD with heat preloading can be a good way to treat soft soil. However, few previous studies have reported related experiments on this topic. Consequently, the relevant calculation model received little attention, which undoubtedly compromises the further engineering practice of the technology. Recently, Li et al. (2023b) proposed a finite strain consolidation model that coupled the self-weight of ultra-soft slurry, soil creep, and changing hydraulic conductivity and compressibility during the consolidation process. However, when applying the heat preloading to soft soil, the thermal elastic viscoplastic constitutive relationship, the effects of temperature on hydraulic conductivity and compressibility, and the heat conduction and convection process cannot be included in Li et al.'s model. Since an effective theoretical model is a valuable guide (Liu et al. 2023a; Liu et al. 2023b; Liu et al. 2022a) to understand the consolidation behaviour and can give sound recommendations for engineering design, the finite strain consolidation model which can take all abovementioned factors into account at the same time, namely fully coupled

finite strain consolidation model, is therefore needed and meaningful to be developed. Normally, such a thermal-hydraulic-mechanical (THM) coupling model is solved by complex numerical methods (Zhang et al. 2021; Zheng et al. 2017). For potential users of the model, these numerical methods are often not readily available for direct use. Hence, a direct and simple GUI that can automatically calculate results after entering basic parameters is accordingly time-saving and necessary for them.

To address the abovementioned issues and fill up the research gaps, this paper aims to propose a fully coupled one-dimensional finite strain consolidation model shown in Figure 1 considering the thermal elastic-viscoplastic characteristics of soft soil as well as a GUI for potential users to conduct relevant consolidation analysis. Besides, physical model tests were designed and conducted to observe the consolidation behaviour and examine the performance of the proposed consolidation model. The modified implicit finite difference method was introduced to solve the nonlinear governing equations and verified with a benchmark case. Furthermore, this paper introduced a factor, namely improvement of consolidation efficiency rate (IER), to study the effect of PHD spacing, externally applied temperature, and thickness of treated soil on consolidation efficiency and give qualitative guidance for the method to be used in practical engineering.

2. Theoretical framework

2.1 Basic assumptions

To expedite the development of the model, it is crucial to establish the following assumptions:

(a) The soil is fully saturated and Darcy's law is applicable;

(b) The temperature range of clay spans from 0°C to 100°C, and the water does not suffer any change in its phase;

(c) Thermal equilibrium is established between the soil particles and the pore water. Both soil particles and pore water exhibit linear expansion as temperature increases;

(d) The influence of temperature on the density of soil particles is neglected.

2.2 Constitutive model

Most recently, Chen and Yin (2023) proposed and verified the one-dimensional thermal elastic-viscoplastic (TEVP) model for the time-dependent behaviour of clays.

$$\begin{aligned}\dot{\varepsilon}_z &= \dot{\varepsilon}_z^{eT} + \dot{\varepsilon}_z^{eM} + \dot{\varepsilon}_z^{vp} \\ &= \frac{\kappa_T}{V}\frac{1}{T}\frac{dT}{dt} + \frac{\kappa}{V}\frac{1}{\sigma'}\frac{d\sigma'}{dt} + \frac{\psi}{Vt_0}\exp\left[-\frac{V}{\psi}\left(\varepsilon-\varepsilon_{zp0}\right)\right]\cdot\left(\frac{\sigma'}{\sigma'_{zp0}}\right)^{\frac{\lambda}{\psi}}\cdot\left(\frac{T}{T_0}\right)^{\frac{\lambda_T}{\psi}}\end{aligned} \tag{1}$$

where the total strain rate of clay consists of three parts: a mechanical elastic strain rate $\dot{\varepsilon}_z^{eM}$, a thermal elastic strain rate $\dot{\varepsilon}_z^{eT}$, and a visco-plastic strain rate $\dot{\varepsilon}_z^{vp}$, T is current

temperature and T_0 is room temperature, σ' is current effective stress, σ'_{zp0} is pre-consolidation pressure of soil, and ε_{zp0} is the strain under σ'_{zp0} on normal compression line, t_0 is reference time, t_e is equivalent time, and V is specific volume of the soil. λ is the normal compression index, κ is the recompression index, κ_T is cooling and reheating index describing the thermal elastic behaviour, λ_T is virgin heating compression index.

The creep of soil is reflected by the visco-plastic strain rate item. The visco-plastic strain rate $\dot{\varepsilon}_z^{vp}$ shown in Eq.(2) is derived based on the concept of equivalent time lines developed by Yin and Graham (1994). By introducing the creep index ψ, reference time t_0, and equivalent time t_e, the creep-related strain can therefore be considered and calculated. The detailed derivation process and explanation can be found in previous studies (Chen et al. 2023a) and will not be repeated here.

$$\dot{\varepsilon}_z^{vp} = \frac{\psi}{Vt_0}\exp\left[-\frac{V}{\psi}\left(\varepsilon-\varepsilon_{zp0}\right)\right]\cdot\left(\frac{\sigma'}{\sigma'_{zp0}}\right)^{\frac{\lambda}{\psi}}\cdot\left(\frac{T}{T_0}\right)^{\frac{\lambda_T}{\psi}} \tag{2}$$

When using the void ratio to express the one-dimensional thermal elastic-viscoplastic model, Eq.(1) is equivalent to

$$\dot{e} = -\kappa_T\frac{\dot{T}}{T}-\kappa\frac{\dot{\sigma}}{\sigma}-\frac{\psi}{t_0}\exp\left(\frac{e-e_{zp0}}{\psi}\right)\left(\frac{\sigma'_z}{\sigma'_{zp0}}\right)^{\frac{\lambda}{\psi}}\cdot\left(\frac{T}{T_0}\right)^{\frac{\lambda_T}{\psi}} \tag{3}$$

where e_{zp0} is the void ratio related to σ'_{zp0}, (σ'_{zp0}, e_{zp0}) is the stress point that lies on the reference time line.

For very soft soil with the initial effective stress close to 0 kPa (Li et al. 2023b), Eq.(3) needed to be modified. Otherwise, the void rate shown in Eq.(3) will tend to be

infinite. In addition, it has been shown that there is a nearly linear relationship between the void ratio e and the logarithm of effective stress σ' throughout a wide range of void ratios (Li et al. 2023b) for different types of soft soil, indicating the validity of extending the one-dimensional TEVP model to finite strain analyses. The modifications are expressed as:

$$\begin{gathered}\Delta e^{e}=-\kappa \ln\left(\frac{\sigma_{ref}^{'}+\sigma'}{\sigma_{ref}^{'}}\right), \Delta e^{Te}=-\kappa_{T} \ln\left(\frac{T}{T_{0}}\right) \\ \Delta e^{ep}=-\lambda \ln\left(\frac{\sigma_{ref}^{'}+\sigma'}{\sigma_{ref}^{'}+\sigma_{zp0}^{'}}\right), \Delta e^{Tep}=-\lambda_{T} \ln\left(\frac{T}{T_{0}}\right) \\ \Delta e_{creep}=-\psi \ln\left(\frac{t_{0}+t_{e}}{t_{0}}\right)\end{gathered} \tag{4}$$

where $\sigma_{ref}^{'}$ is a non-zero small value, which can be taken as 0 to 1 kPa or checked by fitting test data at very small vertical stress.

Based on the above modification, the one-dimensional TEVP model is revised as the extended one-dimensional TEVP model for finite strain, as shown in Figure 2 and Eq.(5)

$$\dot{e}=-\kappa_{T} \frac{1}{T} \frac{dT}{dt}-\kappa \frac{1}{\sigma_{ref}^{'}+\sigma'} \frac{d\sigma'}{dt}-\frac{\psi}{t_{0}} \exp\left(\frac{e-e_{zp0}}{\psi}\right) \cdot\left(\frac{\sigma_{ref}^{'}+\sigma'}{\sigma_{ref}^{'}+\sigma_{zp0}'}\right)^{\frac{\lambda}{\psi}} \cdot\left(\frac{T}{T_{0}}\right)^{\frac{\lambda_{T}}{\psi}} \tag{5}$$

The effective stress principle is formulated as

$$\sigma=\sigma^{'}+u_{w} \tag{6}$$

By incorporating the effective stress principle, Eq.(5) can also be expressed in the following alternative form:

$$\frac{\partial e}{\partial t}=-\kappa_{T} \frac{1}{T} \frac{dT}{dt}-\kappa \frac{\partial\left(\sigma-u_{w}\right) / \partial t}{\sigma_{ref}^{'}+\left(\sigma-u_{w}\right)}-\frac{\psi}{t_{0}} \exp\left(\frac{e-e_{zp0}}{\psi}\right) \cdot\left(\frac{\sigma_{ref}^{'}+\left(\sigma-u_{w}\right)}{\sigma_{ref}^{'}+\sigma_{zp0}'}\right)^{\frac{\lambda}{\psi}} \cdot\left(\frac{T}{T_{0}}\right)^{\frac{\lambda_{T}}{\psi}} \tag{7}$$

186

187 **2.3 Finite strain consolidation process**

188 As shown in Figure 3, the following relationship can be derived according to the

189 law of conservation of mass

190 $$\rho_s(T_0)\left[\Delta a \cdot 1 \cdot (1-n_0)\right] = \rho_s(T)\left[\Delta \xi \cdot 1 \cdot (1-n)\right] \tag{8}$$

191 in which n is the void porosity at time t, and n_0 is the initial void porosity.

192 Hence, the transformation relationship between the Lagrangian and convective

193 coordinate systems in the finite strain thermal consolidation model is as follows:

194 $$\frac{\partial a}{\partial \xi} = \frac{1-n}{1-n_0} \cdot \frac{\rho_s(T)}{\rho_s(T_0)} \tag{9}$$

195 in which $\rho_s(T)$ and $\rho_s(T_0)$ are the density of soil particles at temperature T and

196 room temperature T_0, respectively.

197 It can be seen that compared to the transformation relation between the Lagrangian

198 and convective coordinate systems given by Gibson et al. (1981), the coordinate

199 transformation relation in the finite strain thermal consolidation model has an additional

200 term $\frac{\rho_s(T)}{\rho_s(T_0)}$, which reflects the influence of the effect of heating. Due to the very

201 limited effect on soil particles induced by temperature in the range of 20°C to 60°C

202 (referenced by Eq.(16) and the typical value of α_s ,

203 $\rho_s(20°C)/\rho_s(60°C) = 1+3\cdot10^{-5}\cdot40 = 1.0012$), $\frac{\rho_s(T)}{\rho_s(T_0)}$ can be regarded as 1 in the

204 following derivation.

When examining an element ABCD at time t, which has altered from the original element $A_0B_0C_0D_0$ at time t_0, the vertical force equilibrium of a soil particle can be expressed as

$$\frac{\partial \sigma}{\partial \xi} = \gamma_m = \frac{G_s + e}{1 + e}\gamma_w = \frac{G_s + e}{1 + e}\rho_w g \tag{10}$$

where σ is the total vertical stress, γ_m is the current unit weight of saturated soil, G_s is the specific gravity of the soil particle, γ_m is the unit weight of water, and ρ_w is the density of water at temperature T.

Based on the equilibrium of the pore water, the mathematical expression can be expressed as

$$u_w = u_e + u_h \tag{11}$$

$$\frac{\partial u_w}{\partial \xi} = \frac{\partial u_e}{\partial \xi} + \gamma_w \tag{12}$$

where u_w is the total pore water pressure, u_e is the excess pore water pressure, and u_h is the hydrostatic pressure.

The volume change of the slice $\Delta\xi$ during the following dt time must be equal to the net water volume flowed in or out plus the increase or decrease in the volume of the soil due to the change of temperature. Hence, we have

$$-\frac{\partial}{\partial t}\left(n \cdot \Delta\xi\right)dt = -\left[n\Delta\xi\alpha_w\Delta T + \left(1-n\right)\Delta\xi\alpha_s\Delta T\right] + \frac{\partial}{\partial a}\left[-\frac{k_v}{\gamma_w}\left(\frac{\partial a}{\partial \xi}\frac{\partial u_w}{\partial a} - \gamma_w\right)dt\right]\Delta a \tag{13}$$

where α_w and α_s are coefficients of linear expansion for pore water and soil particles, respectively, n is void porosity, k_v is the permeability coefficient under void ratio e and

225 temperature T, and will be introduced later.

226 Substituting $\Delta\xi$ in Eq.(8) into Eq.(13) by employing assumption (d), the local
227 formula of mass conservation is obtained as follows in terms of the Lagrangian
228 coordinate system.

229

230 $$-\frac{\partial}{\partial t}\left(n\cdot\frac{\partial\xi}{\partial a}\right)=-\frac{1}{1+e_0}\frac{\partial e}{\partial t}=-\left[n\frac{\partial\xi}{\partial a}\alpha_w\frac{dT}{dt}+(1-n)\frac{\partial\xi}{\partial a}\alpha_s\frac{dT}{dt}\right]+\frac{\partial}{\partial a}\left[-\frac{k_v}{\gamma_w}\left(\frac{\partial a}{\partial\xi}\frac{\partial u_w}{\partial a}-\gamma_w\right)\right]$$

231 (14)

232 When applying heat preloading, it is important to consider the effects of
233 temperature change on the change in permeability coefficient. The temperature
234 variations change the viscosity of the water and the density of the water, thus affecting
235 the coefficient of permeability of the soil. The permeability coefficient of the soil at
236 temperature T can be expressed by employing the Kozeny-Carman equation (Abuel-
237 Naga et al. 2007; Campanella and Mitchell 1968; Chen et al. 2017; Deng et al. 2022;
238 Li et al. 2023a):

239 $$k_v(e,T)=k_v(e,T_0)\frac{\rho_w(T)\mu(T_0)}{\rho_w(T_0)\mu(T)} \tag{15}$$

240 where $k_v(e,T)$ and $k_v(e,T_0)$ are permeability coefficient at temperature T and room
241 temperature T_0 under void ratio e, respectively; $\mu(T)$ and $\mu(T_0)$ are the viscosity
242 coefficient of water at temperature T and room temperature T_0, respectively; $\rho_w(T)$
243 and $\rho_w(T_0)$ are the density of pore water at temperature T and room temperature T_0,
244 respectively.

On the one hand, with the definition of the coefficient of linear expansion of soil particles and pore water, the relationship between strain increment and temperature increment can be written as

$$d\varepsilon_w = \alpha_w dT, d\varepsilon_s = \alpha_s dT \tag{16}$$

Since the mass of pore water or soil particles remains constant before and after thermal expansion, the following formulation can therefore be obtained:

$$\rho_w(T_0)/\rho_w(T) = 1+\alpha_w dT, \rho_s(T_0)/\rho_s(T) = 1+\alpha_s dT \tag{17}$$

On the other hand, the coefficient of viscosity of water at one atmospheric pressure as a function of temperature has been given as follows by Yin et al. (2014):

$$\mu(T) = -0.454\times10^{-3}\ln T + 2.349\times10^{-3} \tag{18}$$

Moreover, the relationship between the void ratio and permeability coefficient based on the previous studies (Liu et al. 2018; Zhao and Gong 2019)

$$e = e_k + C_k \lg\left[k_v(e,T_0)/k_v(e_k,T_0)\right] \tag{19}$$

where C_k is the permeability change index.

Combined Eq.(15) to Eq.(19), the following equation holds. It is worth noting that the following k_v refer to $k_v(e,T)$, if not further specified

$$k_v(e,T) = k_v(e_k,T_0)\cdot 10^{\frac{e-e_k}{C_k}} \cdot \frac{\rho_w(T)\mu(T_0)}{\rho_w(T_0)\mu(T)} \tag{20}$$

It shall be noticed that there are two patterns in the relationship between the vertical strain ε and void ratio e, the first is in the convective coordinates called natural strain:

$$\varepsilon_n = \ln \frac{1+e_0}{1+e} \tag{21}$$

The second one is called engineering strain in the Lagrangian coordinate system and is presented as follows:

$$\varepsilon_e = \frac{e_0 - e}{1+e_0} \tag{22}$$

Hence, rewritten Eq.(14), the strain rate in the Lagrangian coordinate system can be expressed as

$$\frac{\partial \varepsilon}{\partial t} = -\frac{1}{1+e_0}\frac{\partial e}{\partial t} = \frac{\partial}{\partial a}\left[-\frac{k_v}{\rho_w g}\left(\frac{1+e_0}{1+e}\frac{\partial u_w}{\partial a} - \gamma_w\right)\right] - a_v \frac{1+e}{1+e_0}\cdot\frac{\partial T}{\partial t} \tag{23}$$

where α_v is the thermal expansion coefficient of saturated soil, $\alpha_v = (1-n)\alpha_s + n\alpha_w$.

Combining Eqs.(7), (14) and (23), the governing equation can be obtained as follows

$$\frac{\partial}{\partial a}\left[\frac{k_v}{\rho_w g}\left(\frac{1+e_0}{1+e}\frac{\partial u_w}{\partial a} - \gamma_w\right)\right] + a_v \frac{1+e}{1+e_0}\cdot\frac{\partial T}{\partial t} =$$

$$-\frac{\kappa_T}{V}\frac{\dot{T}}{T+273.15} - \frac{\kappa}{V}\frac{\partial\left(\sigma - u_w\right)/\partial t}{\sigma'_{ref} + \left(\sigma - u_w\right)} - \frac{\psi}{Vt_0}\exp\left[-\frac{V}{\psi}\left(\varepsilon - \varepsilon_{zp0}\right)\right]\cdot\left(\frac{\sigma'_{ref} + \left(\sigma - u_w\right)}{\sigma'_{ref} + \sigma'_{zp0}}\right)^{\frac{\lambda}{\psi}}\cdot\left(\frac{T+273.15}{T_0+273.15}\right)^{\frac{\lambda_T}{\psi}} \tag{24}$$

The stress expressed in conductive coordinate (i.e., Eq.(10)) can be rewritten in the form of Lagrangian coordinate

$$\frac{\partial \sigma}{\partial a} = \frac{G_s + e}{1+e_0}\gamma_w \tag{25}$$

To express governing equations using excess pore water pressure, a new variable is defined here

$$\sigma = \sigma_{ah} + u_h \tag{26}$$

where σ_{ah} is the total stress above hydrostatic pressure.

Therefore, the effective stress can be expressed as:

$$\sigma^{'} = \sigma_{ah} - u_e \tag{27}$$

Using u_e, σ_{ah} instead of u_w, σ respectively, Eqs.(24) and (25) could be expressed as.

$$\frac{\partial \sigma_{ah}}{\partial a} = \frac{G_s - 1}{1 + e_0}\gamma_w \tag{28}$$

$$\frac{\partial}{\partial a}\left[\frac{k_v}{\rho_w g}\left(\frac{1+e_0}{1+e}\frac{\partial u_e}{\partial a}\right)\right] + a_v \frac{1+e}{1+e_0}\cdot\frac{\partial T}{\partial t} =$$

$$-\frac{\kappa_T}{V}\frac{\dot{T}}{T+273.15} - \frac{\kappa}{V}\frac{\partial\left(\sigma_{ah}-u_e\right)/\partial t}{\sigma'_{ref}+\left(\sigma_{ah}-u_e\right)} - \frac{\psi}{Vt_0}\exp\left(\frac{e-e_{zp0}}{\psi}\right)\cdot\left(\frac{\sigma'_{ref}+\left(\sigma_{ah}-u_e\right)}{\sigma'_{ref}+\sigma'_{zp0}}\right)^{\frac{\lambda}{\psi}}\cdot\left(\frac{T+273.15}{T_0+273.15}\right)^{\frac{\lambda_T}{\psi}} \tag{29}$$

At any given time *t*, the settlement *S* of saturated soft soil is

$$S(t) = \int_0^H \frac{e_0 - e}{1+e_0}da - \int_0^H \alpha_u\left[T\left(a,t\right) - T\left(a,0\right)\right]\frac{1+e}{1+e_0}da \tag{30}$$

where α_u is the thermal expansion coefficient of the soil skeleton.

2.4 Heat conduction and convection process

The internal energy change of the slice $\Delta\xi$ during the following dt time must be equal to the net heat flow in or out plus the decrease in the internal energy of the water due to the net outflows. On the one hand, the internal energy change shown in Figure 3 of the slice $\Delta\xi$ during dt can be written as:

$$-\frac{\partial E}{\partial t}dt = -\frac{\partial}{\partial t}\left[C_s\rho_s\left(T\right)\left(1-n\right)\Delta\xi\left(T-T_0\right) + C_w\rho_w\left(T\right)n\Delta\xi\left(T-T_0\right)\right]dt \tag{31}$$

301 in which C_w and C_s are the specific heat capacity of pore water and soil particles,

302 respectively.

303 On the other hand, the internal energy change induced by thermal conductivity

304 shown in Figure 3 can be expressed as:

305 $$\Delta E = \frac{\partial}{\partial a}\left[\dot{Q}(a)\,dt\right]\Delta a \tag{32}$$

306 Using Fourier's law of thermal conductivity (Incropera et al. 1996), Eq.(32) can

307 be rewritten as:

308 $$\begin{aligned}\Delta E = \frac{\partial}{\partial a}\left[\dot{Q}(a)\,dt\right]\Delta a &= \frac{\partial}{\partial a}\left\{\left(-n\lambda_w\frac{\partial T}{\partial \xi}-(1-n)\lambda_s\frac{\partial T}{\partial \xi}\right)dt\right\}\Delta a \\ &= \frac{\partial}{\partial a}\left\{-\left[(1-n)\lambda_s + n\lambda_w\right]\frac{\partial T}{\partial \xi}\,dt\right\}\Delta a\end{aligned} \tag{33}$$

309 where λ_w and λ_s are the thermal conductivity of pore water and soil particles,

310 respectively.

311 The internal energy of the water due to the net outflows can be presented as:

312 $$\Delta E = \frac{\partial}{\partial a}\left\{C_w\rho_w(T)v_w(a)\,dt\left(T-T_0\right)\right\}\Delta a \tag{34}$$

313 Combining Eqs.(31), (33) and (34), the governing conservation equation of

314 energy can be expressed as:

315 $$\begin{aligned}&\frac{\partial}{\partial t}\left[C_s\rho_s(T)(1-n)\Delta\xi\left(T-T_0\right)+C_w\rho_w(T)n\Delta\xi\left(T-T_0\right)\right]dt = \\ &-\frac{\partial}{\partial a}\left\{-\left[(1-n)\lambda_s+n\lambda_w\right]\frac{\partial T}{\partial \xi}\,dt\right\}\Delta a-\frac{\partial}{\partial a}\left\{C_w\rho_w(T)v_w\,dt\left(T-T_0\right)\right\}\Delta a\end{aligned} \tag{35}$$

316 The water velocity in Eq.(35) can be expressed from Eq.(12)

317 $$v_w = -\frac{k_v}{\rho_w(T)g}\frac{1+e_0}{1+e}\frac{\partial u_e}{\partial a} \tag{36}$$

318 Since there is no change in the mass of the soil during the consolidation process,

the following relationship holds.

$$\frac{\partial\left[\rho_s(T)(1-n)\Delta\xi\right]}{\partial t}=0 \tag{37}$$

The mass change of water can be expressed by

$$-\frac{\partial}{\partial t}\left(\rho_w(T)\cdot n\cdot\frac{\Delta\xi}{\Delta a}\right)=\frac{\partial}{\partial a}\left(\rho_w(T)\cdot v_w\right) \tag{38}$$

Based on Eqs.(35)-(38), the governing equation can be developed as:

$$\left(\frac{C_s\rho_s(T_0)}{1+e_0}+\frac{C_w\rho_w(T)e}{1+e_0}\right)\frac{\partial T}{\partial t}=\frac{\partial}{\partial a}\left\{\left[\lambda_s(1-n)+\lambda_w n\right]\frac{1+e_0}{1+e}\frac{\partial T}{\partial a}\right\}-C_w\rho_w(T)q_w\frac{\partial T}{\partial a} \tag{39}$$

2.5 Initial and boundary conditions

At t=0, the excess pore water pressure is linearly distributed along the depth of the soil due to the self-weight stress. The temperature inside the soil is room temperature, so the initial condition can be written as

$$\begin{aligned} u_e(a,0)&=\frac{G_s-1}{1+e_0}\gamma_w a \\ T(a,0)&=T_0 \end{aligned} \tag{40}$$

The temperature at the bottom heated PHD increases linearly to T_1 and then remains constant, as shown in Figure 4. The change in temperature against time can be expressed as:

$$A(t)=\begin{cases} T_0+\Delta T\cdot t/t_d & (0\le t\le t_d) \\ T_1 & (t>t_d) \end{cases} \tag{41}$$

where ΔT is temperature increment, $\Delta T=T_1-T_0$; T_0 represents the initial temperature of

saturated clay, and t_d means heating time.

In practice, step-by-step pressurization is usually adopted to prevent soil particles from clogging when vacuum pressure is applied. A multi-step vacuum loading, say 5-step loading shown in Figure 5 can be expressed as follows. Other forms of multi-stage vacuum loading applied at the bottom of the soil can be given similar expressions.

$$p(t)=\begin{cases} P_1, 0 \le t < t_1 \\ P_2, t_1 \le t < t_2 \\ P_3, t_2 \le t < t_3 \\ P_4, t_3 \le t < t_4 \\ P_5, t \ge t_4 \end{cases} \tag{42}$$

where P_i $(i=1,2,3,4,5)$ is vacuum loading at different stages, t_i $(i=1,2,3,4)$ is the applied time of each level of vacuum loading.

The top boundary conditions of saturated clay can be obtained as:

$$\begin{aligned} u_e(0,t)&=0 \\ T(0,t)&=T_0 \end{aligned} \tag{43}$$

According to the temperature loading and vacuum pressures applied at the bottom of the soil, the bottom boundary conditions can be written as:

$$\begin{aligned} u_e(H,t)&=-p(t) \\ T(H,t)&=A(t) \end{aligned} \tag{44}$$

2.6 Numerical implementation using FDM

Given the inherent nonlinearity of the governing equations, obtaining an analytical or semi-analytical solution becomes highly challenging. To solve this issue, this paper uses a modified implicit differential format to solve the governing equations. The soil

354 is divided into m (i=1, 2, 3,…, m+1) parts in space, and time is divided into N (k=1, 2,
355 3,…, N+1) parts. In the original differential format, the coefficients of the undetermined
356 variables (i.e., u_e and T) are supposed to be calculated using related parameters from
357 step k+1. The modified differential format linearizes the nonlinear governing equations
358 by employing related parameters from step k to determine these coefficients, which
359 makes the governing equations easy to solve and ensures the accuracy of solutions
360 (Gautschi 2011). The next section will show the reliability of the modified differential
361 format. Figure 6 illustrates the modified difference format in space and time. For
362 Eq.(24), the following equations hold.

363
$$F_{i+1/2}^{k}\frac{u_{i+1}^{k+1}-u_{i}^{k+1}}{\triangle a^{2}}+F_{i-1/2}^{k}\frac{u_{i-1}^{k+1}-u_{i}^{k+1}}{\triangle a^{2}}+G_{i}^{k}\frac{T_{i}^{k+1}-T_{i}^{k}}{\triangle t}=-H_{i}^{k}\frac{T_{i}^{k+1}-T_{i}^{k}}{\triangle t}$$
$$-I_{i}^{k}\frac{\left(\sigma_{ah}\right)_{i}^{k+1}-\left(\sigma_{ah}\right)_{i}^{k}}{\triangle t}+I_{i}^{k}\frac{u_{i}^{k+1}-u_{i}^{k}}{\triangle t}-g_{i}^{k}\left(u,e,T\right) \tag{45}$$

364 and

365
$$k_{v,i}^{k}=k_{vr,R}\cdot\Psi\left(T_{i}^{k}\right)\cdot10^{\left(e_{i}^{k}-e_{r}\right)/C_{k}} \tag{46}$$

366
$$\left(\sigma_{ah}\right)_{i+1}^{k}=\left(G_{s}-1\right)/\left(1+e_{0}\right)\rho_{w,i}^{k}\Delta a+\left(\sigma_{ah}\right)_{i}^{k} \tag{47}$$

367
$$F_{i\pm1/2}^{k}=\frac{k_{v,i\pm1/2}^{k}}{\rho_{w,i\pm1/2}^{k}g}\frac{1+e_{i\pm1/2}^{1}}{1+e_{i\pm1/2}^{k}} \tag{48}$$

368
$$G_{i}^{k}=\left[\left(1-n_{i}^{k}\right)\alpha_{s}+n_{i}^{k}\alpha_{w}\right]\frac{1+e_{i}^{k}}{1+e_{i}^{1}} \tag{49}$$

369
$$H_{i}^{k}=\frac{\kappa_{T}}{1+e_{i}^{1}}\frac{1}{\left(T_{i}^{k}+273.15\right)} \tag{50}$$

370
$$I_{i}^{k}=\frac{\kappa}{1+e_{i}^{1}}\frac{1}{\sigma'_{ref}+\left(\sigma_{ah}\right)_{i}^{k}-u_{i}^{k}} \tag{51}$$

371 $$g_i^k\left(u,e,T\right)=\frac{\psi}{t_0\left(1+e_i^1\right)}\exp\left(\frac{e_i^k-e_{zp0}}{\psi}\right)\left(\frac{\sigma'_{ref}+\left(\sigma_{ah}\right)_i^k-u_i^k}{\sigma'_{ref}+\sigma'_{zp0}}\right)^{\frac{\lambda}{\psi}}\left(\frac{T_i^k+273.15}{T_0+273.15}\right)^{\frac{\lambda_T}{\psi}} \quad (52)$$

372 where

$$\rho_{w,i\pm1/2}^k=\left(\rho_{w,i}^k+\rho_{w,i\pm1}^k\right)/2,\rho_{w,i}^k=\rho_{wR}/\left[1+\alpha_w\left(T_i^k-T_0\right)\right],\rho_{s,i\pm1/2}^k=\left(\rho_{s,i}^k+\rho_{s,i\pm1}^k\right)/2$$

373 $$\rho_{s,i}^k=\rho_{sR}/\left[1+\alpha_s\left(T_i^k-T_0\right)\right],e_{i\pm1/2}^k=\left(e_i^k+e_{i\pm1}^k\right)/2,k_{v,i\pm1/2}^k=\left(k_{v,i}^k+k_{v,i\pm1}^k\right)/2$$

$$\Psi\left(T_i^k\right)=\left[\rho_{w,i}^k\cdot\mu_i\left(T_i^1\right)\right]\Big/\left[\rho_{w,i}^1\cdot\mu_i\left(T_i^k\right)\right],n_i^k=e_i^k/\left(1+e_i^k\right),i=1,2,3,...,m+1$$

374 The initial condition can be written as

375 $$u_i^1=0\ \left(i=1,2,...,m+1\right) \quad (53)$$

376 The upper and bottom boundaries for excess pore water pressure can be presented

377 as

378 $$\begin{aligned}u_1^k&=0\\u_{m+1}^k&=P^k\end{aligned} \quad (54)$$

379 $$P^k=\begin{cases}P_1,0\le n<n_{d1}\\P_2,n_{d1}\le n<n_{d2}\\P_3,n_{d2}\le n<n_{d3}\\P_4,n_{d3}\le n<n_{d4}\\P_5,n\ge n_{d4}\end{cases} \quad (55)$$

380 in which $n_d=\frac{t_d}{\Delta t},n_{di}=\frac{t_i}{\Delta t}\ (i=1,2,3,4)$.

381 For governing Eq.(39), the following differential format can be presented.

382 $$W_i^k\frac{T_i^{k+1}-T_i^k}{\triangle t}=X_{i+1/2}^k\frac{T_{i+1}^{k+1}-T_i^{k+1}}{\triangle a^2}+X_{i-1/2}^k\frac{T_{i-1}^{k+1}-T_i^{k+1}}{\triangle a^2}-Y_i^k\frac{T_{i+1}^{k+1}-T_{i-1}^{k+1}}{2\triangle a} \quad (56)$$

383 where

384 $$W_i^k=C_s\frac{\rho_{s,i}^1}{1+e_i^0}+C_w\rho_{w,i}^k\frac{e_i^k}{1+e_i^1} \quad (57)$$

385 $$X_{i\pm1/2}^k=\left(\frac{\lambda_s}{1+e_{i\pm1/2}^k}+\frac{\lambda_w\cdot e_{i\pm1/2}^k}{1+e_{i\pm1/2}^k}\right)\frac{1+e_{i\pm1/2}^1}{1+e_{i\pm1/2}^k} \quad (58)$$

386 $$Y_i^k = C_w \rho_{w,i}^k q_{w,i}^k \tag{59}$$

387 $$q_{w,i}^k = -\frac{k_{v,i}^k}{\rho_{w,i}^k g}\frac{1+e_i^1}{1+e_i^j}\frac{u_{i+1}^k - u_{i-1}^k}{2\Delta a} \tag{60}$$

388 The initial thermal condition and thermal boundary conditions can be written as:

389 $$T_i^1 = T_0 \ \ (i = 1, 2, 3, ..., m+1) \tag{61}$$

390 $$\begin{aligned} T_1^k &= T_0 \\ T_{m+1}^k &= A^k \end{aligned} \tag{62}$$

391 with

392 $$A^k = \begin{cases} T_0 + \Delta T \cdot n / n_d & \left(0 \le n \le n_d\right) \\ T_1 & \left(n > n_d\right) \end{cases} \tag{63}$$

393 in which $n_d = \frac{t_d}{\Delta t}$.

394 Combining Eqs.(45) to (63), a numerical program has been made to predict the
395 consolidation behaviour through Matlab software.

396 **3. Verification with the benchmark case**

397 Pu et al. (2018) proposed a benchmark case for a one-dimensional finite strain
398 consolidation model considering the self-weight stress of soil and used the piecewise
399 linearized numerical technique (Fox and Berles 1997; Liu et al. 2022b) to solve the
400 consolidation model. When the temperature increases at the bottom boundary is not
401 considered, i.e., $\Delta T = 0$, the consolidation model proposed in this paper can be degraded
402 to the benchmark problem proposed by Pu et al. (2018). The parameters employed for
403 verification are taken from Pu et al. (2018) and listed in Table 1.

404 The distribution of excess pore water pressure and void ratio at *t*= 0.1, 1, and 2

405 years against the height of soil under double-drained and sigle-drained boundaries were
406 plotted in Figure 7 and Figure 8, respectively. It can be seen from the figures that the
407 calculated values of excess pore water pressure and void ratio from this paper show
408 great agreement with the benchmark case. The comparison with the benchmark case
409 indicates that the modified finite difference method proposed in this paper is correct
410 and reliable.

411 **4. Model performance**

412 To further examine the validity of the model, the proposed consolidation model
413 and the modified finite difference method are used to predict the consolidation
414 behaviour of three physical model tests (i.e., PM1, PM2, and PM3). The configuration
415 of each part of the physical model box, the placement of the sensors, the mounting of
416 the heating PHD, etc. can be seen in Figure 9. Detailed schematic and dimensional
417 information can be found in Figure 10. Figure 11 shows the initial setup of the physical
418 model and the initial state of the slurry. The slurry used in the physical model was
419 bentonite slurry taken from a disposal site in Hong Kong. According to the result of the
420 X-ray diffraction (XRD) test, the tested soil contained 15% montmorillonite, 10%
421 feldspar, 43% quartz, and 32% other minerals. The soil consists of 17% clay, 68% silt,
422 and 15% sand. The liquid limit, plastic limit, and plastic index of the soil are 86%, 27%,
423 and 59%, respectively. To consider the initial state of the slurry after the use in
424 construction projects, the soil was thoroughly mixed with water to obtain the slurry with

425 about 300% water content, which is 3.5 times the liquid limit of the slurry. During the
426 consolidation process, the slurry samples at various heights were taken from the
427 sampling holes on the wall of the model tank for water content measurement. There is
428 a well-accepted relationship (Craig 2013) between void, water content, and saturation:

429 $$S_r = \frac{wG_s}{e} \tag{64}$$

430 where S_r is the saturation of soil, w is water content, G_s is specific gravity, and e is the
431 void ratio.

432 The slurry is considered fully saturated during the consolidation process, meaning
433 S_r equals 1. In addition, the specific gravity G_s is measured to be 2.63 in three physical
434 models. Therefore, the void ratio can be obtained by measuring the water content at
435 different heights and times and used for examining the performance of the proposed
436 consolidation model. According to the test data of three physical models, the
437 temperature at the bottom boundary always remains unchanged during the
438 consolidation process, so it is reasonable to regard the physical boundary at the bottom
439 as a uniform heating boundary. By equalizing the vacuum boundary at the bottom
440 boundary based on the principles shown in Figure 12, the consolidation behaviour of
441 three physical model tests can be predicted using the consolidation model proposed in
442 this paper.

443 In PM 1, the bottom heating wire was not energized throughout the consolidation,
444 so the temperature at the bottom remained at room temperature. In PM 2, after 24 hours
445 of self-weight consolidation, the soil began to be heated and continued for 10 hours,

446 with the final bottom temperature maintained at 40℃. In PM3, the soil was heated and
447 continued for 19 hours after 24 hours of self-weight consolidation, and the final bottom
448 temperature was maintained at 60℃. It shall be noticed that the temperature sensor
449 controls a linear increase in the temperature of the heated wire over time. Meanwhile,
450 all of the above three physical models started vacuuming after 2 days, and the vacuum
451 loads were applied continuously in multiple stages to prevent clogging of the PHD. The
452 loading information including thermal loading and vacuum pressure is presented in
453 Figure 13 accordingly. The proposed consolidation model has 15 unknown parameters,
454 including 11 parameters in the one-dimensional TEVP model and 4 parameters related
455 to soil particles and soil skeleton. Eight basic parameters $e_0, \lambda, \kappa, \sigma'_{zp0}, \psi, t_0, \lambda_T, \kappa_T$ can
456 be measured from temperature-controlled odometer tests (Chen et al. 2023a). Three
457 basic parameters e_k, C_k, k_{vT_0} are obtained by adopting back calculation from the
458 oedometer test (Chen et al. 2023b). The rest 4 parameters $\alpha_s, \alpha_u, \lambda_s, C_s$ are referenced
459 from previous studies (Jiang et al. 2023; Liu et al. 2018; Mitchell and Soga 2005; Zhou
460 and Ng 2015). All parameters used in the model application are listed in Table 2.
461 According to the applied temperature and vacuum loading information, the
462 mathematical expressions for heat loading of the three physical models can be written
463 as

$$PM1: T(H,t) = 20^{\circ}C$$

$$PM2: T(H,t) = \begin{cases} 20^{\circ}C, \ 0 \le t < 24h \\ 20^{\circ}C + 2(t-24), \ 24 \le t < 34h \\ 40^{\circ}C, \ t \ge 34h \end{cases} \tag{65}$$

$$PM3: T(H,t) = \begin{cases} 20^{\circ}C, \ 0 \le t < 24h \\ 20^{\circ}C + \frac{40}{19}(t-24), \ 24 \le t < 43h \\ 60^{\circ}C, \ t \ge 43h \end{cases}$$

The mathematical formula for vacuum pressure can be expressed as

$$P(H,t) = \begin{cases} 0 \ kPa, \ 0 \le t < 2 \ days \\ -10 \ kPa, \ 2 \le t < 3 \ days \\ -20 \ kPa, \ 3 \le t < 4 \ days \\ -40 \ kPa, \ 4 \le t < 5 \ days \\ -60 \ kPa, \ 5 \le t < 6 \ days \\ -80 \ kPa, \ 6 \le t \le 30 \ days \end{cases} \tag{66}$$

It should be noted that Eq.(66) is the actual applied vacuum pressure of the physical model, and according to the equivalence principle shown in Figure 12, the actual applied vacuum pressure needs to be multiplied by a discount factor S_1/S_2 in order to be brought into the proposed consolidation model for calculation.

Figure 14 shows the comparison of the measured data of PM1 with the calculation results. Figures 14(a)-(c) present the distribution of void ratio against the height of soil at t=2, 10, and 30 days. It can be found that there is a good agreement between the calculated and measured void ratio at three different times during the consolidation process at room temperature. Figure 14(d) depicts the comparison of measured settlement of soil with calculated values during the whole consolidation process. The maximum difference between the predicted and measured values is within 2 cm, which indicates that there is good agreement between prediction consolidation behaviour with

observed behaviour. Since the vacuum loading was applied after 2 days, the consolidation rate (i.e., the slope of the settlement curve) has a sudden increment. Hence, there is an inflection point in the initial stage of consolidation.

Figure 15 shows the comparison of measured data of PM2 with the calculation results. Figures 15(a)-(c) present the distribution of void ratio along the height of soil at t=2, 10, and 30 days. It shall be noticed that the predicted void ratio with depth of soil has a good match with the measured values at around 10 days. The predicted void ratio in the later stage deviated slightly from the measured ones, which is consistent with the observation that the predicted values of settlement shifted from the predicted values in the later stages of consolidation. During the later stage of consolidation, we assumed that the temperature at the top surface of the soil is room temperature (i.e., boundary condition (43)). However, in the actual heating process, the temperature at the top surface of the soil is higher than 20℃, which leads to the temperature distribution along the depth of soil being higher than the calculated values, and thus the corresponding calculated void ratio is larger than measured ones. Nevertheless, it can still be concluded that the computational model proposed in this paper still has good prediction performance from Figure 15.

Figure 16 shows the comparison of measured data of PM3 with the calculation results. Figures 16(a)-(c) present the distribution of void ratio along the height of soil at t=2, 10, and 30 days. As the temperature at the bottom of PM3 reaches a steady state, the calculated void ratio deviates from the measured ones to a greater extent compared

to the PM2 test. The reason for this phenomenon is similar to the PM2 test, where the top temperature boundary condition is treated in a way that may not match the actual situation. In three physical models, the acrylic model box was covered by a plastic sheet shown in Figure 9, which caused the temperature of the top temperature boundary to exceed room temperature. The difference is that the PM3 test has a higher stabilized temperature at the bottom boundary and a greater deviation of the measured values from the predicted values compared to the PM2 test. Accordingly, the settlement predictions were smaller than the actual values. However, in the engineering application of heating PHD, the thermal insulation of the soil in the field is not as desirable as the physical model tests. The soil surface temperature is supposed to be close to room temperature, and the model proposed in this paper is still very effective. Certainly, a more accurate 2D plane strain or 3D model reflecting the fully coupled thermal consolidation characteristics of soft soil requires further study in the future.

5. Improvement of consolidation efficiency

The results of theoretical calculations and laboratory physical model tests support heating PHD as an effective means of improving soil consolidation efficiency. Quantifying the improvement of efficiency will be useful in guiding the application of the consolidation method. Therefore, the technique of heating PHD to accelerate consolidation is discussed in terms of consolidation efficiency enhancement in this section. IER (improvement of consolidation efficiency rate) is defined in this paper to

quantify the improvement of consolidation efficiency. All parameters used in this section are taken from the PM2 test in Table 2 if no further illustration.

$$IER = \frac{\varepsilon\left(t, H, s_1/s_2, T, P_{vacuum}\right) - \varepsilon\left(t, P_{vacuum}\right)}{\varepsilon\left(t, P_{vacuum}\right)} \tag{67}$$

Figure 17(a) depicts the improvement of consolidation efficiency against time under different applied temperatures. The case without considering heating PHD was used for comparison, and the other parameters were the same as the PM2 test parameters. It can be seen that the effect of temperature on the improvement of consolidation efficiency is significant, and as the applied temperature is higher, IER is greater. For any temperature increase, IER increased with time until a peak value was reached and then decreased. The turning point means that as the pore water in the slurry is drained, the permeability decreases, and the rate of consolidation decreases, but overall it is more efficient than consolidation without heating.

Figure 17(b) depicts the improvement of consolidation efficiency against time under different spacing of PHD. The case with the spacing of PHD equal to 20 cm was used for comparison. As the simplification shown in Figure 12 made in this paper, the ratio of S_1 and S_2 can reflect the spacing of PHD. S_1/S_2 equals 0.7165, 0.7822, and 0.8889 corresponding to the spacing of PHD of 16 cm, 14 cm, and 10 cm, respectively. From the figure, it can be concluded that although the smaller the spacing, the greater the IER, further reduction of spacing of PHD does not contribute much to the efficiency improvement when the spacing is less than 20 cm.

Figure 17(c) depicts the improvement of consolidation efficiency against time

under different initial soil heights. The case with the initial height of soil equal to 1 m was used for comparison. It can be seen that reducing the initial height of the slurry for the heating PHD treatment achieves better efficiency in the early stages of consolidation but has no significant effect in the later stages. For smaller initial soil heights, the diffusion rate of the vacuum at PHD is faster, so the initial consolidation efficiency is higher in the early stage of consolidation. However, in the later stages, for different initial heights of the soil, the strain becomes similar, so the ISR is no longer improved.

6. Graphical user interface

It can be found that the numerical methods used in solving the governing equations are quite complicated for engineers and potential readers. Hence, to facilitate the application of the proposed model in this paper by engineers and researchers, a GUI has been created and compiled into a .exe file for use in relevant engineering projects, as shown in Figure 18. This .exe file can be easily installed, allowing users to input parameters obtained from geotechnical tests and obtain calculation results without any additional operations required. The .exe file can be provided upon request.

7. Conclusions

The primary findings of this paper are succinctly outlined as follows:

(1) This paper established a one-dimensional fully coupled finite strain thermal elastic viscoplastic consolidation model for soft soil treated by prefabricated

560 horizontal drain with vacuum and heat preloading.

561 (2) Since the system of governing equations corresponding to the consolidation
562 model proposed in this paper is highly nonlinear, the modified finite difference
563 method has been employed to solve the model. The correctness and reliability
564 of the numerical method proposed in this paper were illustrated by comparing
565 the degraded calculation results with a benchmark case. Based on the verified
566 numerical method and consolidation model, good performance has been
567 observed in the comparison with three physical experiments.

568 (3) The results of three physical models showed that the settlements of soil were
569 0.34 m, 0.41 m, and 0.54 m at 30 days when the heat preloading was 20℃,
570 40℃, and 60℃, respectively. The calculation results of the proposed model
571 demonstrated that the maximum values of IER were 18.8%, 13.3%, and 7.1%
572 when the heat preloading was 50℃, 40℃, and 30℃, respectively. The
573 maximum values of IER were 8.4%, 6.1%, and 4.5% when the spacing of PHD
574 were 10 cm, 14 cm, and 16 cm, respectively. Furthermore, the values of IER
575 at the early stage of consolidation were 45.5%, 28.0%, and 15.2% when the
576 soil heights were 0.65 m, 0.75 m, and 0.85 m, respectively.

577 (4) To make it easier for engineers and potential researchers to apply the
578 consolidation model proposed in this paper, the consolidation model has been
579 compiled into a .exe file. Engineers and potential researchers can easily apply
580 the consolidation model proposed in this paper to predict the consolidation

behaviour of related projects by simply inputting the appropriate parameters based on the geotechnical tests and loading parameters.

Data Availability Statement

All data, models, or code that support the findings of this study are available from the corresponding author upon reasonable request. Please feel free to contact us for the automatic calculation software if needed.

Conflict of Interests

The authors declare that there is no conflict of interest regarding the publication of this paper.

Acknowledgement

The work presented in this paper is supported by the Research Grants Council (RGC) of Hong Kong Special Administrative Region Government (HKSARG) of China (RIF: R5037-18; GRF: 15210020, 15221721, and 15226722). The authors also acknowledge the financial supports from three grants (CD7A, CD7J, and CD82) from Research Institute for Land and Space from The Hong Kong Polytechnic University.

Appendix I: Notation list

The following notations are adopted in this paper:

a = Lagrangian coordinate

599 C_k = permeability change index

600 C_s = specific heat capacity of soil particle

601 C_w = specific heat capacity of pore water

602 e = void ratio

603 e_0 = initial void ratio

604 e_{zp0} = void ratio related to σ'_{zp0}

605 e_k = void ratio in e-log$k$ curve

606 G_s = specific gravity of the soil particle

607 H = height of soil

608 i = hydraulic gradient

609 k_v = hydraulic conductivity

610 k_{vT0} = vertical hydraulic conductivity at room temperature at e=e_k

611 m = element number in vertical direction

612 N = number of divisions in time dimension

613 n= porosity

614 n_0= initial porosity

615 S = surface settlement

616 T= temperature

617 T_0= room temperature

618 t = time

619 t_d = heating time

620 t_e= equivalent time

621 t_0= reference time

622 u_e = excess pore water pressure

623 u_h = hydrostatic pressure

624 u_w = total pore water pressure

625 V = specific volume

626 v_w = flow velocity of pore water

627 α_s = thermal expansion coefficient of soil particle

628 α_w = thermal expansion coefficient of pore water

629 α_u = thermal expansion coefficient of soil skeleton

630 ρ_s = density of soil particles at temperature T

631 ρ_w = density of pore water at temperature T

632 ρ_{sT_0} = density of soil particles at room temperature

633 ρ_{wT_0} = density of pore water at room temperature

634 γ_w = unit weight of water

635 μ = coefficient of viscosity of water

636 ε = strain

637 ε_{zp0} = strain related to σ'_{zp0}

638 $\dot{\varepsilon}$ = strain rate

639 κ = elastic compression index in the Cam-Clay model

640 κ_T = cooling and reheating index

641 λ = elastic-plastic compression index in the Cam-Clay model

642 λ_T = virgin heating compression index

643 λ_s = thermal conductivity of soil particle

644 λ_w = thermal conductivity of pore water

645 ξ = convective coordinate

646 σ = total stress

647 σ' = effective stress

648 σ'_{zp0} = similar role to the pre-consolidation pressure p_c

649 σ_{ah} = total stress above hydrostatic pressure

650 σ'_{ref} = reference effective stress

651 ψ = creep index

652

Appendix II: Finite difference scheme

The finite difference scheme of the present one-dimensional finite strain thermal consolidation governing equations (45) and (56) can be presented as follows, respectively:

$$AA_i^k u_{i-1}^{k+1} + BB_i^k u_i^{k+1} + CC_i^k u_{i+1}^{k+1} = DD_i^k u_i^k + EE_i^k \left(T_i^{k+1} - T_i^k\right) + FF_i^k \tag{A1}$$

$$GG_i^k T_{i-1}^{k+1} + HH_i^k T_i^{k+1} + II_i^k T_{i+1}^{k+1} = JJ_i^k T_i^k \tag{A2}$$

where

$$AA_i^k = F_{i-1/2}^k \frac{\triangle t}{\triangle a^2}, BB_i^k = \left[-I_i^k - \frac{\triangle t}{\triangle a^2}\left(F_{i+1/2}^k + F_{i-1/2}^k\right)\right], CC_i^k = F_{i+1/2}^k \frac{\triangle t}{\triangle a^2}, DD_i^k = -I_i^k, EE_i^k = -\left(G_i^k + H_i^k\right)$$

$$FF_i^k = -g_i^k\left(u, \varepsilon, T\right)\triangle t, GG_i^k = \left(-X_{i-1/2}^k \frac{\triangle t}{\triangle a^2} - Y_i^k \frac{\triangle t}{2\triangle a}\right), HH_i^k = \left[W_i^k + \frac{\triangle t}{\triangle a^2}\left(X_{i+1/2}^k + X_{i-1/2}^k\right)\right]$$

$$II_i^k = \left(Y_i^k \frac{\triangle t}{2\triangle a} - X_{i+1/2}^k \frac{\triangle t}{\triangle a^2}\right), JJ_i^k = W_i^k$$

Applying boundary conditions, the above governing equations can be expressed in matrix form as follows:

$$\begin{bmatrix} BB_2^k & CC_2^k & & & \\ AA_3^k & BB_3^k & CC_3^k & & \\ \vdots & & \ddots & & \\ & & AA_{m-1}^k & BB_{m-1}^k & CC_{m-1}^k \\ & & & AA_m^k & BB_m^k \end{bmatrix} \begin{bmatrix} u_2^{k+1} \\ u_3^{k+1} \\ \vdots \\ u_{m-1}^{k+1} \\ u_m^{k+1} \end{bmatrix} = \begin{bmatrix} DD_2^k \cdot u_2^k \\ DD_3^k \cdot u_3^k \\ \vdots \\ DD_{m-1}^k \cdot u_{m-1}^k \\ DD_m^k \cdot u_m^k - CC_m^k \cdot u_{m+1}^k \end{bmatrix} + \begin{bmatrix} EE_2^k\left(T_2^{k+1} - T_2^k\right) \\ EE_3^k\left(T_3^{k+1} - T_3^k\right) \\ \vdots \\ EE_{m-1}^k\left(T_{m-1}^{k+1} - T_{m-1}^k\right) \\ EE_m^k\left(T_m^{k+1} - T_m^k\right) \end{bmatrix} + \begin{bmatrix} FF_2^k \\ FF_3^k \\ \vdots \\ FF_{m-1}^k \\ FF_m^k \end{bmatrix} \tag{A3}$$

667
$$\begin{bmatrix} HH_2^k & II_2^k & & & \\ GG_3^k & HH_3^k & II_3^k & & \\ \vdots & & \ddots & & \\ & & GG_{m-1}^k & HH_{m-1}^k & II_{m-1}^k \\ & & & GG_m^k & HH_m^k \end{bmatrix} \begin{bmatrix} T_2^{k+1} \\ T_3^{k+1} \\ \vdots \\ T_{m-1}^{k+1} \\ T_m^{k+1} \end{bmatrix} = \begin{bmatrix} JJ_2^k \cdot T_2^k + GG_2^k \cdot T_0 \\ JJ_3^k \cdot T_3^k \\ \vdots \\ JJ_{m-1}^k \cdot T_{m-1}^k \\ JJ_m^k \cdot T_m^k - II_m^k \cdot T_{m+1}^k \end{bmatrix} \quad \text{(A4)}$$

668 After incorporating the initial conditions, the updated temperature and excess pore

669 water pressure can be therefore obtained.

670 **References**

671 Abuel-Naga, H.M., Bergado, D., Bouazza, A., and Ramana, G. (2007). "Volume change
672 behaviour of saturated clays under drained heating conditions: experimental
673 results and constitutive modeling". *Canadian Geotechnical Journal*, 44(8): 942-
674 956.
675 Abuel-Naga, H.M., Bergado, D., and Chaiprakaikeow, S. (2006). "Innovative thermal
676 technique for enhancing the performance of prefabricated vertical drain during
677 the preloading process". *Geotextiles and Geomembranes*, 24(6): 359-370.
678 Artidteang, S., Bergado, D., Saowapakpiboon, J., Teerachaikulpanich, N., and Kumar,
679 A. (2011). "Enhancement of efficiency of prefabricated vertical drains using
680 surcharge, vacuum and heat preloading". *Geosynthetics International*, 18(1):
681 35-47.
682 Biot, M.A. (1956). "Thermoelasticity and irreversible thermodynamics". *Journal of*
683 *Applied Physics*, 27(3): 240-253.
684 Britto, A., Savvidou, C., Maddocks, D., Gunn, M., and Booker, J. (1989). "Numerical
685 and centrifuge modelling of coupled heat flow and consolidation around hot
686 cylinders buried in clay". *Géotechnique*, 39(1): 13-25.
687 Campanella, R.G., and Mitchell, J.K. (1968). "Influence of temperature variations on
688 soil behavior". *Journal of the Soil Mechanics and Foundations Division*, 94(3):
689 709-734.
690 Chen, W., Ma, Y., Yu, H., Li, F., Li, X., and Sillen, X. (2017). "Effects of temperature
691 and thermally-induced microstructure change on hydraulic conductivity of
692 Boom Clay". *Journal of Rock Mechanics and Geotechnical Engineering*, 9(3):
693 383-395.
694 Chen, Z.-J., Feng, W.-Q., Chen, W.-B., and Yin, J.-H. (2023a). "A thermal elastic visco-
695 plastic model for soft clayey soils". *Canadian Geotechnical Journal*, 61(2):
696 208-227.
697 Chen, Z.-J., Feng, W., Li, A., Al-Zaoari, K.Y.M., and Yin, J.-H. (2023b). "Experimental
698 and molecular dynamics studies on the consolidation of Hong Kong marine
699 deposits under heating and vacuum preloading". *Acta Geotechnica*, 18(5):

2569-2583.
Chen, Z.-j., Li, P.-l., Li, A., Yin, J.-h., and Song, D.-b. (2024). "New simple method for calculating large-strain consolidation settlement of layered soft soils with horizontal drains and vacuum preloading with comparison to test data". *Geotextiles and Geomembranes*, 52(4): 725-735.
Chen, Z.-J., and Yin, J.-H. (2023). "A New One-Dimensional Thermal Elastic-Viscoplastic Model for the Thermal Creep of Saturated Clayey Soils". *Journal of Geotechnical and Geoenvironmental Engineering*, 149(4): 04023010.
Cheng, T., Yan, K., Zheng, J.-J., Luo, X.-F., Zhang, D.-B., Xu, W.-H., Hu, R.-J., and Zhang, Y. (2017). "Semi-analytical and semi-numerical method for the single soil layer consolidation problem". *Engineering Computations*, 34(3): 960-987.
Chiba, T., Shinsha, H., and Tani, Y. 1992. Development of a vacuum-consolidation method employing horizontal drains. Japan Dredging and Reclamation Engineering Association, Tokyo (Japan).
Chu, J., Guo, W., and Yan, S. (2011). "Geosynthetic tubes and geosynthetic mats: Analyses and applications". *Geotechnical Engineering*, 42(1): 57.
Craig, R.F. 2013. Soil mechanics. Springer.
Deng, Y.-b., Mao, W.-y., Yu, L., Zhu, Y.-h., and Xie, K.-h. (2022). "Consolidation and creep coupling model for soft soil considering temperature effect". *Engineering Mechanics*, 39(8): 103-113.
Du, C., Hu, X., Fu, H., and Wang, J. (2021). "Effects of temperature circulation on dredged sludge improved by vacuum preloading". *Soils and Foundations*, 61(5): 1343-1353.
Fox, P.J., and Berles, J.D. (1997). "CS2: A piecewise-linear model for large strain consolidation". *International Journal for numerical and analytical methods in geomechanics*, 21(7): 453-475.
Fredlund, D.G., and Hasan, J.U. (1979). "One-dimensional consolidation theory: unsaturated soils". *Canadian Geotechnical Journal*, 16(3): 521-531.
Gautschi, W. 2011. Numerical analysis. Springer Science & Business Media.
Geng, X., and Yu, H.-S. (2017). "A large-strain radial consolidation theory for soft clays improved by vertical drains". *Géotechnique*, 67(11): 1020-1028.
Gibson, R.E., Schiffman, R.L., and Cargill, K.W. (1981). "The theory of one-dimensional consolidation of saturated clays. II. Finite nonlinear consolidation of thick homogeneous layers". *Canadian Geotechnical Journal*, 18(2): 280-293.
Guo, W., Chu, J., and Yan, S. Deformation of slurry filled permeable geosynthetic tubes. *In* Geo-congress 2013: Stability and performance of slopes and embankments III. 2013. pp. 34-43.
Incropera, F.P., DeWitt, D.P., Bergman, T.L., and Lavine, A.S. 1996. Fundamentals of heat and mass transfer. Wiley New York.
Jiang, W., Feng, C., Ge, S., Fu, S., and Li, J. (2023). "Fully coupled model for one-dimensional large-strain consolidation and heat conduction in saturated clay". *Journal of Engineering Mechanics*, 149(4): 04023014.

Li, A., Chen, Z.-J., Feng, W.-Q., and Yin, J.-H. (2023a). "The Effects of Temperature on One-Dimensional Consolidation and Creep Behaviors of Hong Kong Marine Deposits". *International Journal of Geomechanics*, 23(12): 04023215.

Li, P., Yin, J.-H., Yin, Z.-Y., and Chen, Z. (2023b). "One–dimensional nonlinear finite strain analysis of self–weight consolidation of soft clay considering creep". *Computers and Geotechnics*, 153: 105081.

Liu, Q., Deng, Y.-B., and Wang, T.-Y. (2018). "One-dimensional nonlinear consolidation theory for soft ground considering secondary consolidation and the thermal effect". *Computers and Geotechnics*, 104: 22-28.

Liu, Y., Zheng, J.-J., Zhao, X., and You, L. (2023a). "Analytical model for two-dimensional electro-osmosis-enhanced preloading consolidation of unsaturated soil". *Acta Geotechnica*, 18(2): 1093-1110.

Liu, Y., Zheng, J.J., and Lu, J.T. (2023b). "An analytical model for 2D consolidation of unsaturated soil with semi-permeable boundaries considering self-weight stress and time-dependent loading". *International Journal for Numerical and Analytical Methods in Geomechanics*, 47(6): 903-935.

Liu, Y., Zheng, J.J., Zhao, X., Cao, W., and Huang, Z. (2022a). "A closed-form solution for axisymmetric electro-osmotic consolidation considering smear effects". *Acta Geotechnica*, 17(6): 2597-2609.

Liu, Y., Zheng, J.J., Zhao, X.D., Lu, J.T., and Huang, Z.F. (2022b). "Piecewise-Linear Model for Large-Strain Consolidation with Threshold Hydraulic Gradient". *International Journal of Geomechanics*, 22(5): 06022005.

Mitchell, J.K., and Soga, K. 2005. Fundamentals of soil behavior. John Wiley & Sons New York.

Pu, H., Song, D., and Fox, P.J. (2018). "Benchmark problem for large strain self-weight consolidation". *Journal of Geotechnical and Geoenvironmental Engineering*, 144(5): 06018002.

Pu, H.F., Wang, K., Qiu, J.W., and Chen, X.L. (2020). "Large-strain numerical solution for coupled self-weight consolidation and contaminant transport considering nonlinear compressibility and permeability". *Applied Mathematical Modelling*, 88: 916-932.

Saowapakpiboon, J., Bergado, D., and Artidteang, S. (2011). "Comparison on the performance of prefabricated vertical drain (PVD) preloading combined with and without vacuum and heat". *Lowland Technology International*, 13(1, June): 2-9.

Saowapakpiboon, J., Bergado, D., Thann, Y., and Voottipruex, P. (2009). "Assessing the performance of prefabricated vertical drain with vacuum and heat preloading". *Geosynthetics International*, 16(5): 384-392.

Terzaghi, K. (1923). "Die Berechnung der Durchlassigkeitsziffer des Tones aus Dem Verlauf der Hidrodynamichen Span-nungserscheinungen Akademie der Wissenschaften in Wien". *Mathematish-Naturwissen-Schaftiliche Klasse*, 132: 125-138.

784 Terzaghi, K. (1943). "Theoretical Soil Mechanics". 265-296.
785 Vrakas, A., and Anagnostou, G. (2015). "A simple equation for obtaining finite strain
786 solutions from small strain analyses of tunnels with very large convergences".
787 *Géotechnique*, 65(11): 936-944.
788 Wang, J., Cai, Y., Yuan, G., Fu, H., Sun, W., Hu, X., Wang, P., and Ni, J. (2020).
789 "Temperature effects on dredged slurry performance under vacuum preloading".
790 *Canadian Geotechnical Journal*, 57(12): 1970-1981.
791 Yin, J.-H., and Graham, J. (1994). "Equivalent times and one-dimensional elastic
792 viscoplastic modelling of time-dependent stress–strain behaviour of clays".
793 *Canadian Geotechnical Journal*, 31(1): 42-52.
794 Yin, T., LIU, G., and GUO, Z. (2014). "Theoretical and experimental study on thermal
795 consolidation characteristics of typical soft clay in Ningbo region". *Building*
796 *Structure*, 44(8): 66-69.
797 Zhang, H., Sun, H.-l., Liu, S.-j., Chu, J., Shi, L., Geng, X.-y., Deng, Y.-f., and Cai, Y.-
798 q. (2023a). "Large-Strain Consolidation of Sludge in Multiple-Drainage
799 Geotextile Tubes". *Journal of Geotechnical and Geoenvironmental Engineering*,
800 149(6): 04023037.
801 Zhang, H., Sun, H., Liu, S., Geng, X., Deng, Y., and Cai, Y. (2023b). "Combined
802 vacuum-assisted geotextile and geomembrane tubes for sludge dewatering: A
803 theoretical switching point". *Canadian Geotechnical Journal*,(ja).
804 Zhang, H., Wang, W.-j., Liu, S.-j., Chu, J., Sun, H.-l., Geng, X.-y., and Cai, Y.-q. (2022).
805 "Consolidation of sludge dewatered in geotextile tubes under combined fill and
806 vacuum preloading". *Journal of Geotechnical and Geoenvironmental*
807 *Engineering*, 148(6): 04022032.
808 Zhang, Z., Masum, S.A., Tian, G., and Thomas, H.R. (2021). "Modelling non-
809 isothermal volume change and solute transport behaviours of a semi-permeable
810 clay soil under the combined influence of mechanical loading, chemical-
811 osmosis, and thermo-osmosis". *Engineering Geology*, 293: 106271.
812 Zhao, X.-D., Liu, Y., and Gong, W.-H. (2020). "Analytical solution for one-dimensional
813 electro-osmotic consolidation of double–layered system". *Computers and*
814 *Geotechnics*, 122: 103496.
815 Zhao, X.D., and Gong, W.H. (2019). "Model for large strain consolidation with non-
816 Darcian flow described by a flow exponent and threshold gradient".
817 *International Journal for Numerical and Analytical Methods in Geomechanics*,
818 43(14): 2251-2269.
819 Zheng, L., Rutqvist, J., Xu, H., and Birkholzer, J.T. (2017). "Coupled THMC models
820 for bentonite in an argillite repository for nuclear waste: Illitization and its effect
821 on swelling stress under high temperature". *Engineering Geology*, 230: 118-129.
822 Zhou, C., and Ng, C.W.W. (2015). "A thermomechanical model for saturated soil at
823 small and large strains". *Canadian Geotechnical Journal*, 52(8): 1101-1110.

824

825

Figure Captions

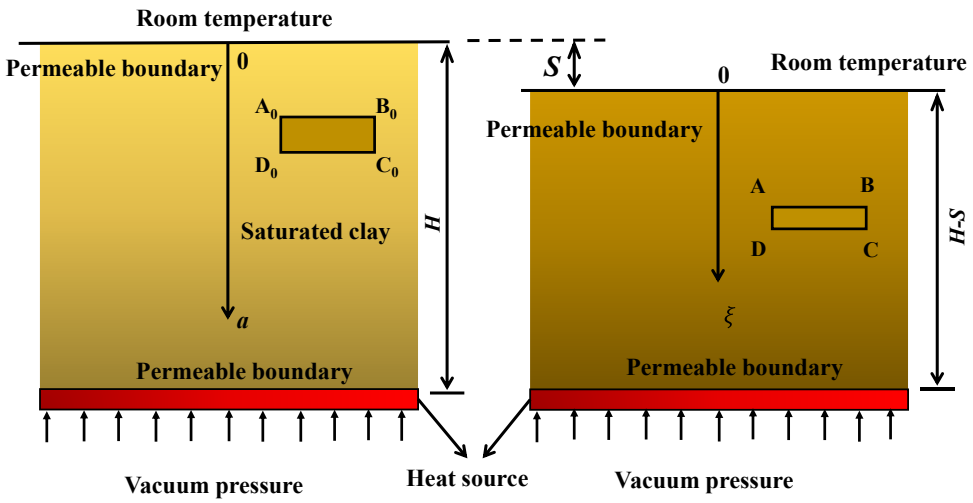

861

862 Figure 1. Schematic diagram of the fully coupled one dimensional thermal

863 consolidation model considering creep

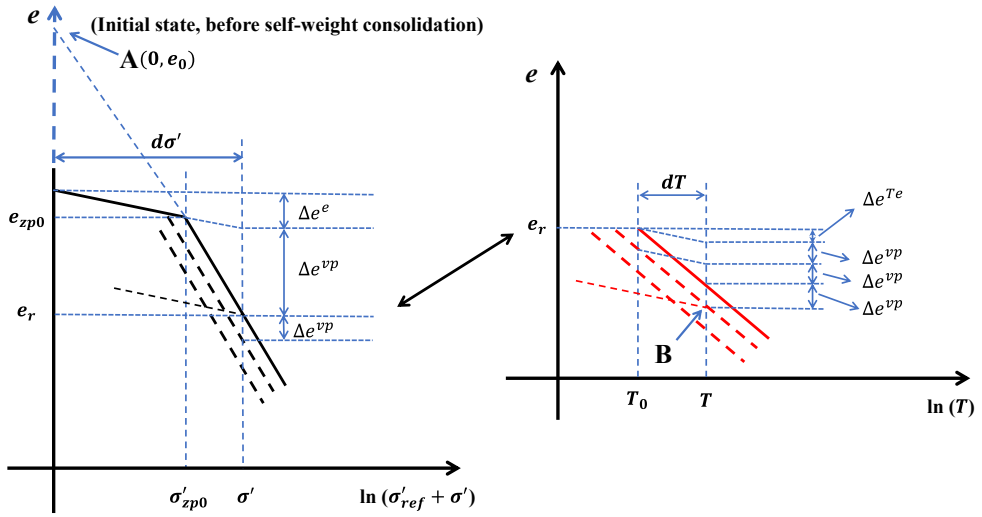

864

865 Figure 2. Extended one dimensional TEVP model for finite strain consolidation

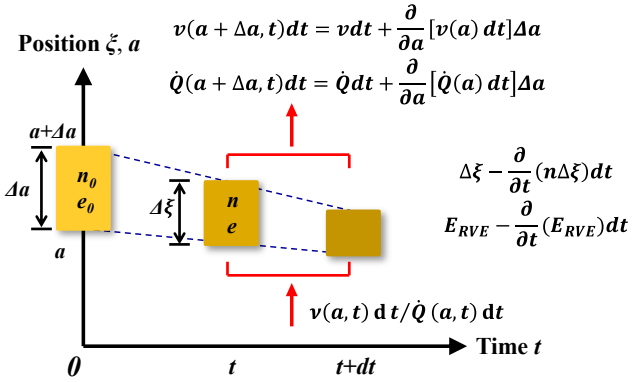

866

867 Figure 3. Mass conservation of the water and heat flow passing through the

868 skeleton section between two skeleton points in an RVE

869

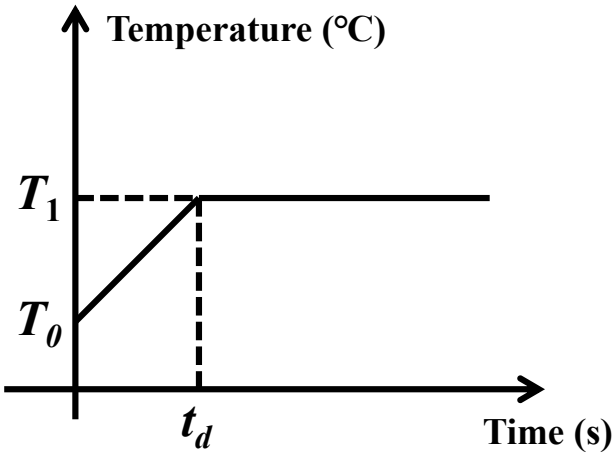

870

871 Figure 4. Schematic diagram of temperature change of heated prefabricated horizontal

872 drainage

873

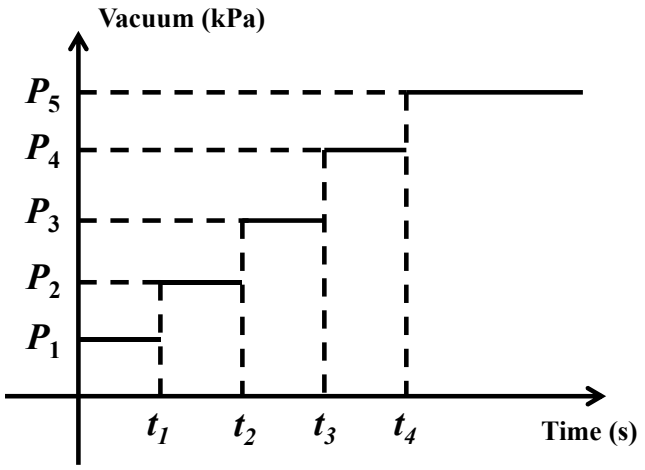

874

875 Figure 5. Schematic diagram of vacuum loading applied to the bottom of the soil

876

877

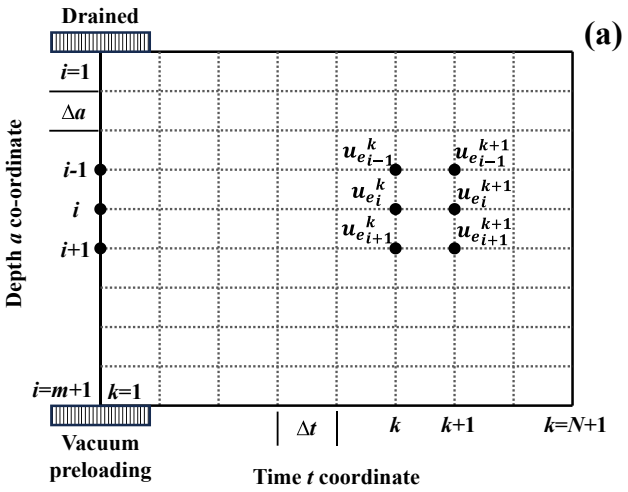

878

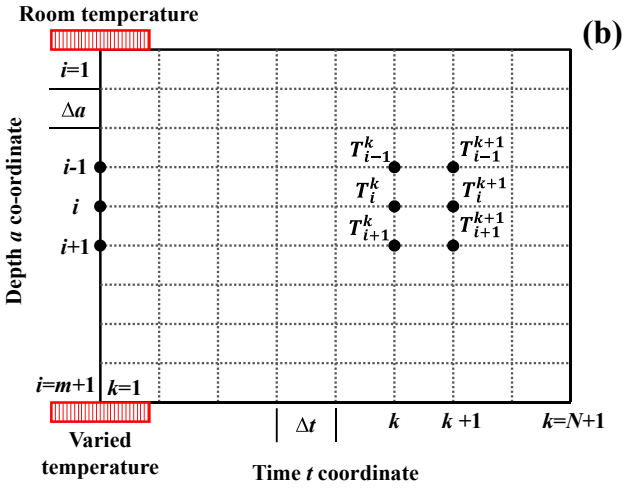

879 Figure 6. Finite difference grid and boundary information of: (a) excess pore water

880 pressure and (b) temperature

881

882

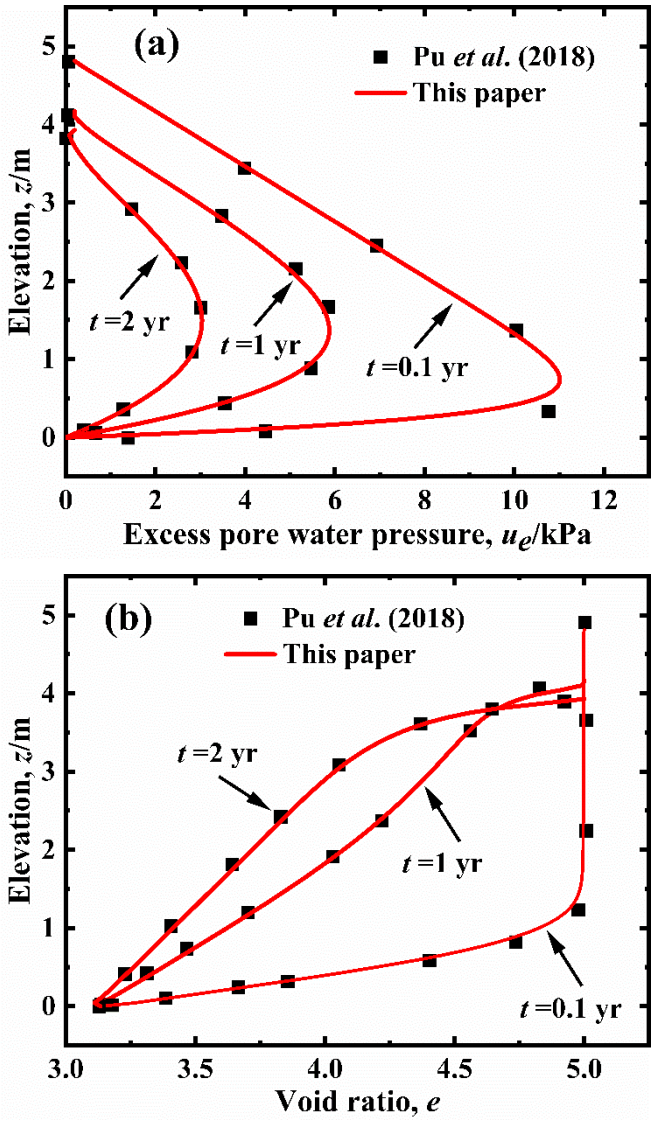

883

884 Figure 7. Comparison of calculation values and the results of Pu et al. (2018)

885 under double-drained boundary: (a) excess pore water pressure and (b) void ratio

886

887

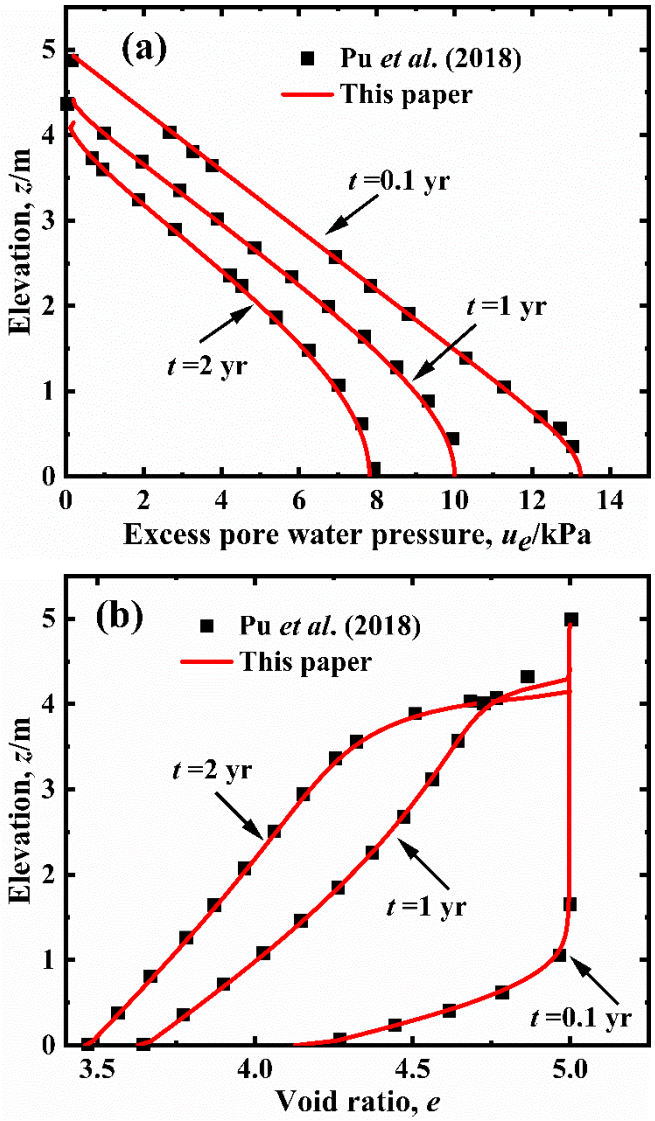

888

889 Figure 8. Comparison of calculation values and the results of Pu et al. (2018)

890 under single-drained boundary: (a) excess pore water pressure and (b) void ratio

891

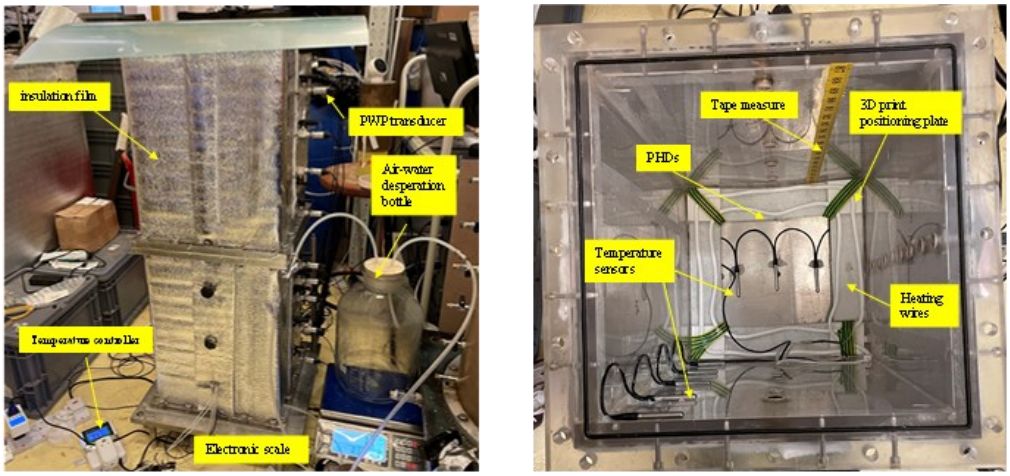

892

893 Figure 9. Front view and top view of the physical model

894

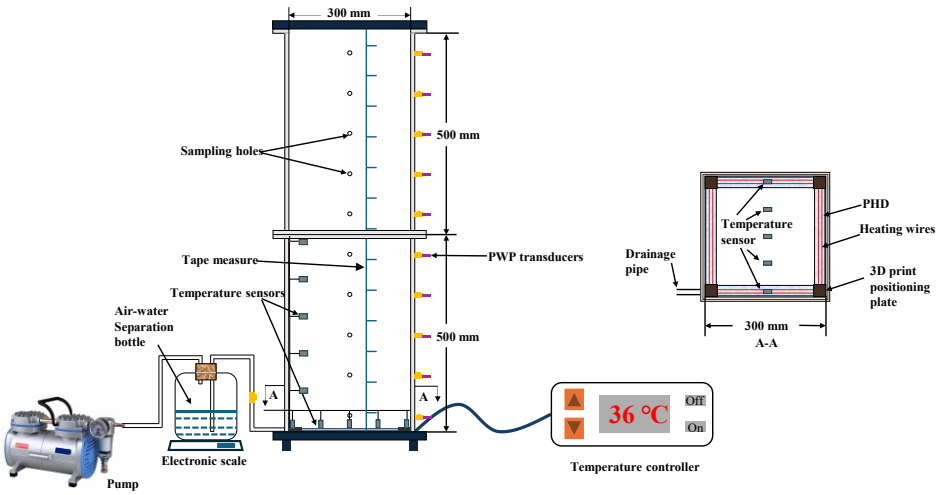

895

896 Figure 10. Schematic diagram of the physical model

897

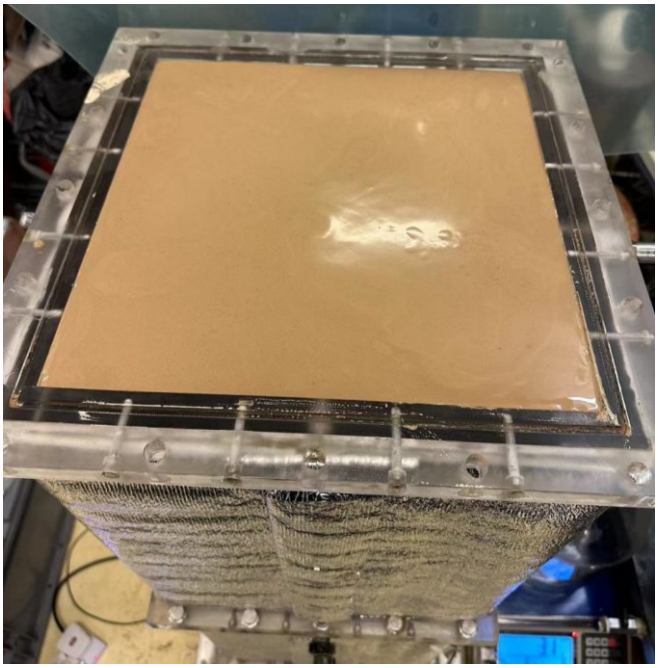

Figure 11. Physical model setup and initial state of slurry

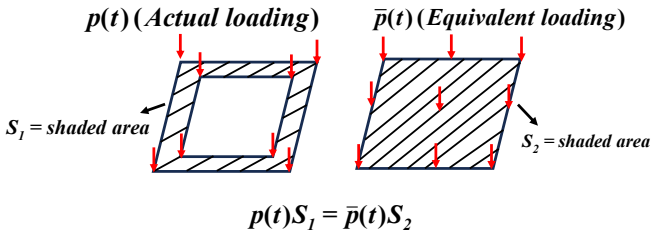

901

902 Figure 12. Schematic diagram of the principle of vacuum pressure equivalence

903

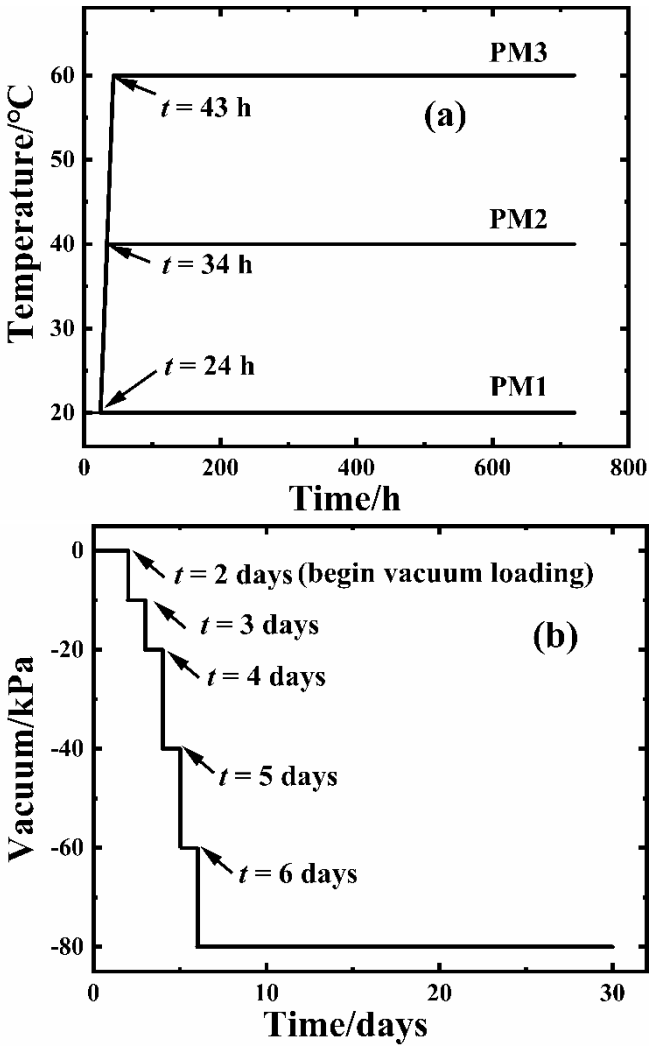

Figure 13. The applied temperature and vacuum loading at the bottom boundary versus time: (a) temperature and (b) vacuum

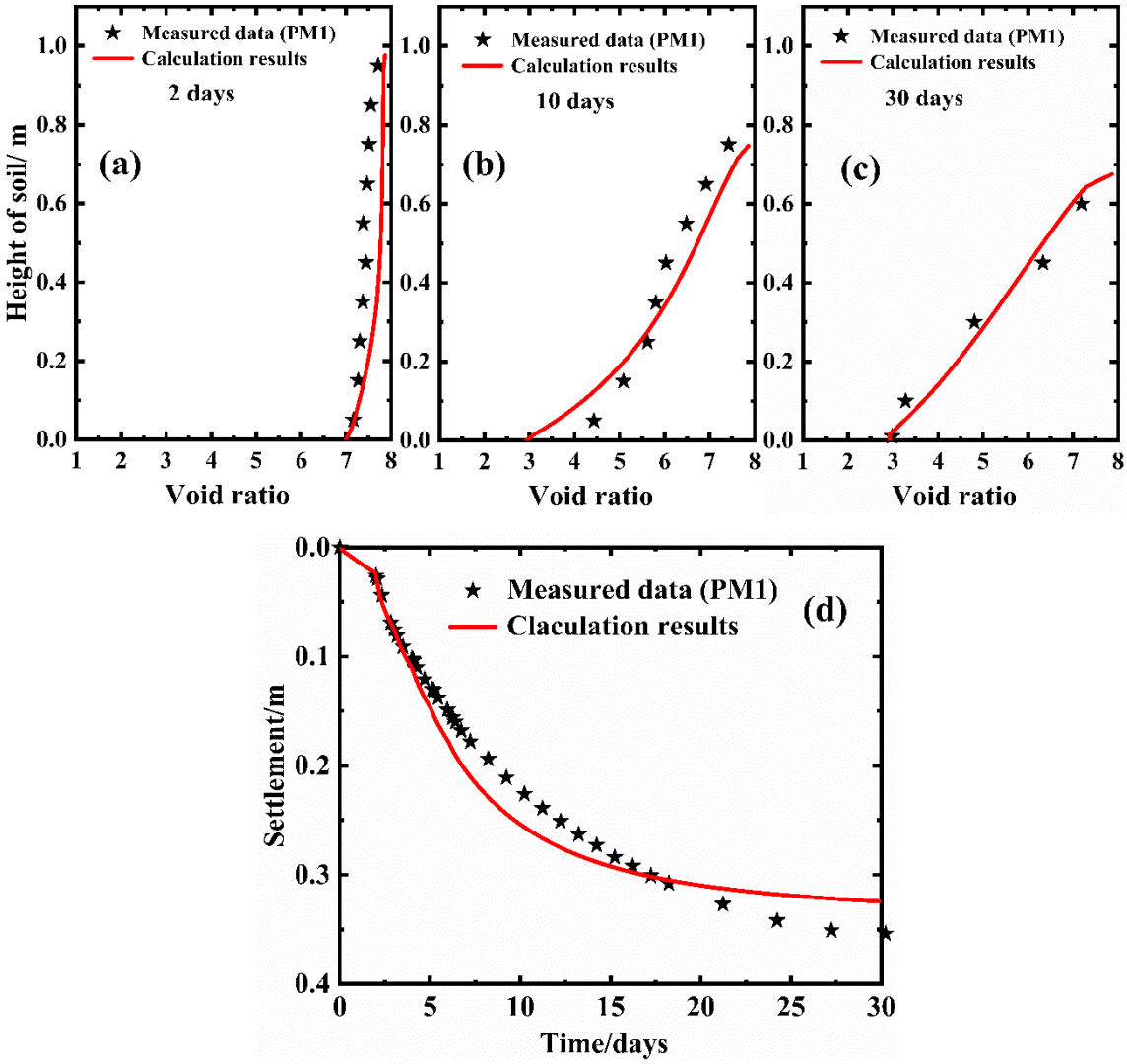

909

910

911 Figure 14. Comparison of measured data with calculation results of PM1: (a)

912 void ratio at t=2 days; (b) void ratio at t=10 days; (c) void ratio at t=30 days; and (d)

913 surface settlement

914

915

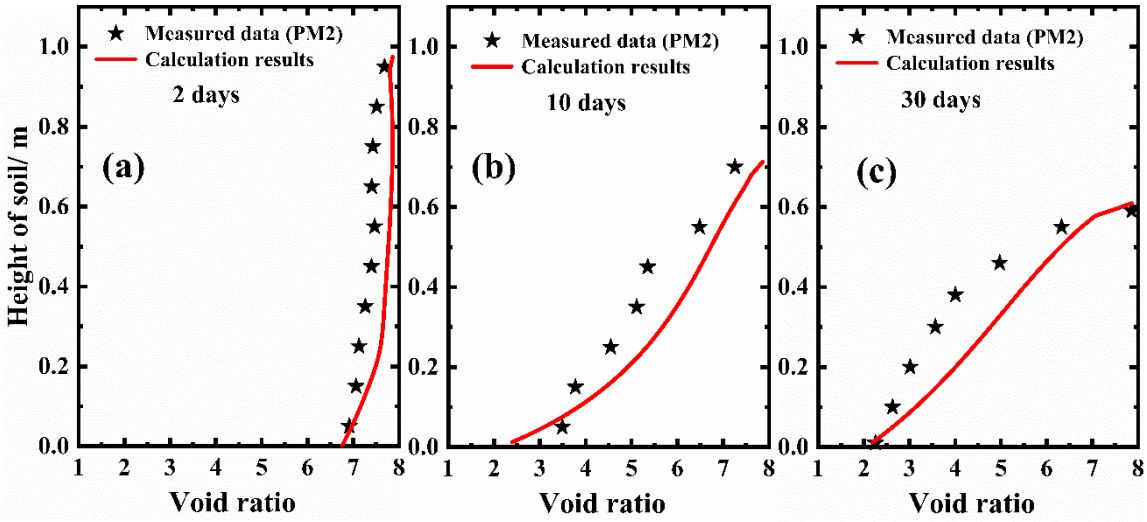

916

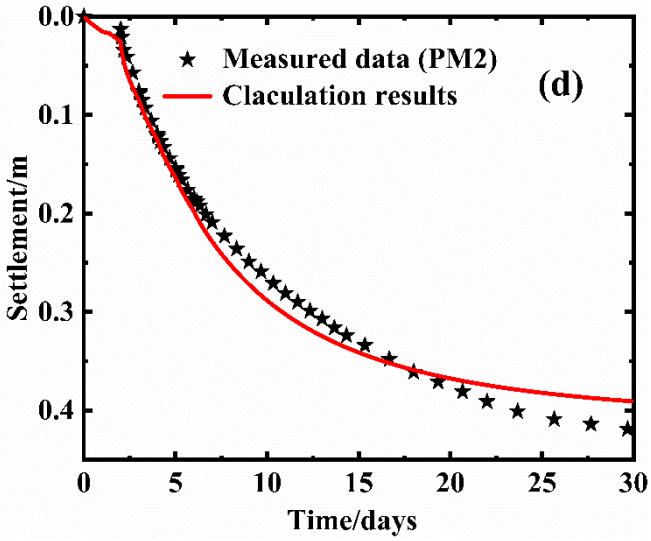

917 Figure 15. Comparison of measured data and calculation results of PM2: (a) void

918 ratio at *t*=2 days; (b) void ratio at *t*=10 days; (c) void ratio at *t*=30 days; and (d)

919 surface settlement

920

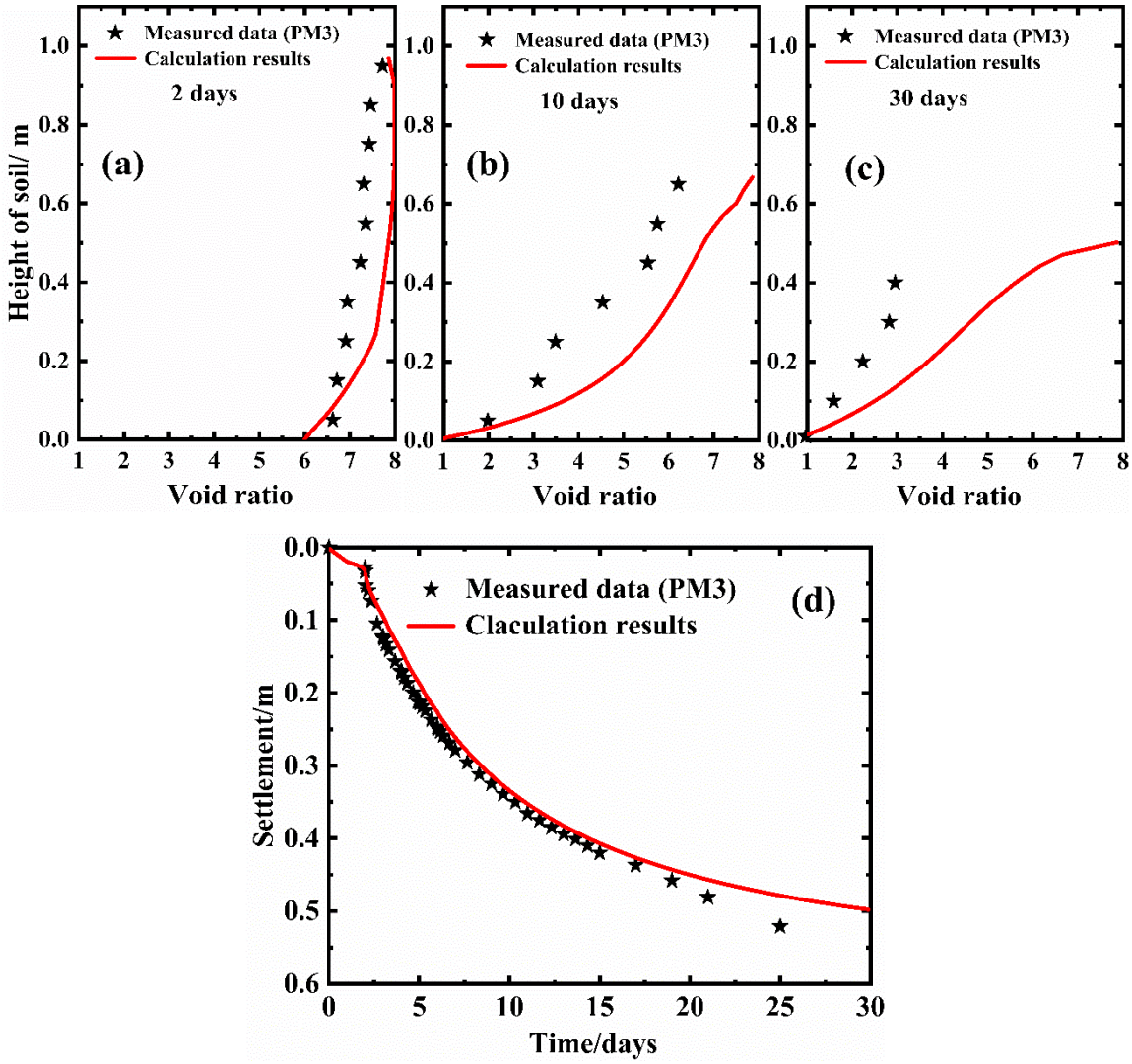

921

922

923 Figure 16. Comparison of measured data and calculation results of PM3: (a) void

924 ratio at *t*=2 days; (b) void ratio at *t*=10 days; (c) void ratio at *t*=30 days; and (d)

925 surface settlement

926

927

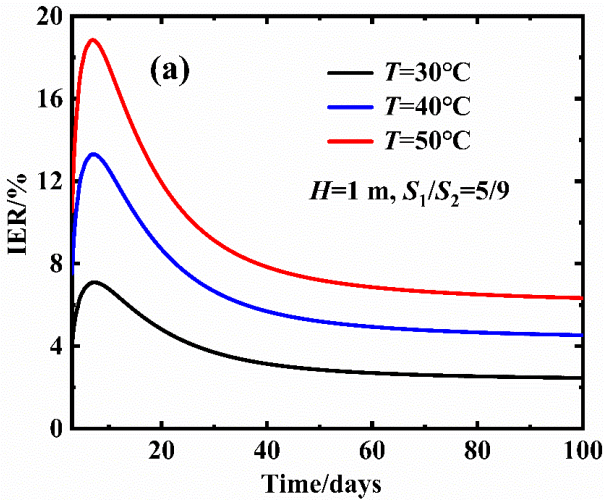

928

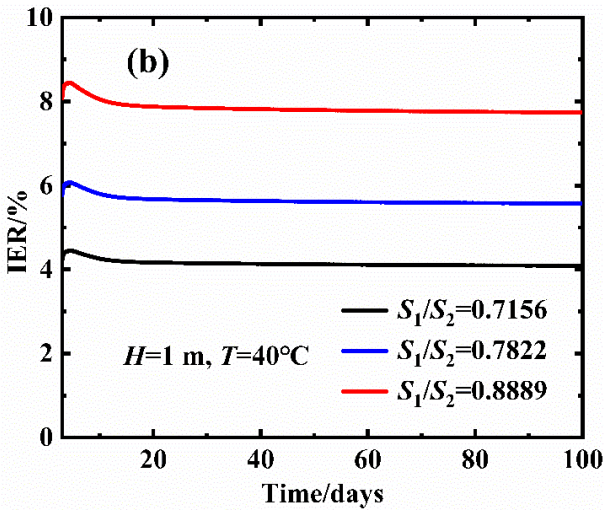

929

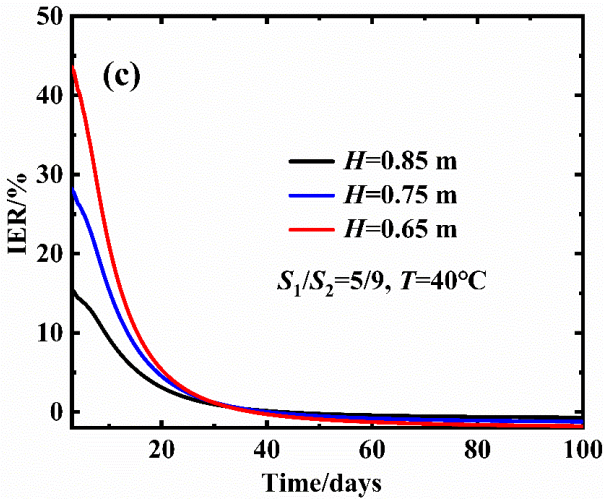

930 Figure 17. Improvement of consolidation efficiency with time under different:

931 (a) heating temperature; (b) spacing of heating PHD; and (c) initial height of

932 slurry

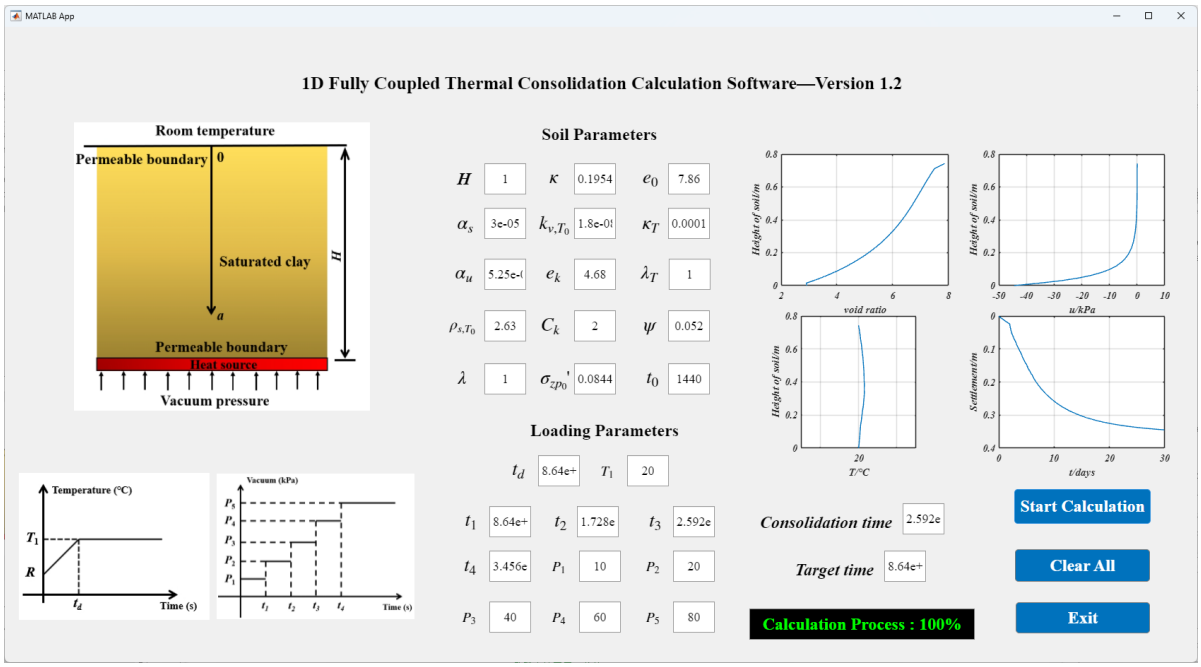

Figure 18. The interface of the automatic calculation software

937 Table 1. Parameters for verification (after Pu et al. (2018))

Parameters	Values	Units
H	5	m
G_s	2.78	-
e_0	5.0	-
e_k	4.3	-
C_k	1.3	-
k_v	2.0×10^{-8}	m/s
κ	0.005	-
λ	0.4343	-
ψ	0.0217	-
σ'_{zp0}	0.2	kPa
σ'_{ref}	0.0013	kPa
t_0	100	day

938

939 Table 2. Parameters of three physical models

Parameters	PM1	PM2	PM3	Units
H	1	1	1	m
α_s	3.0×10^{-5}	3.0×10^{-5}	3.0×10^{-5}	1/℃
α_w	3.5×10^{-4}	3.5×10^{-4}	3.5×10^{-4}	1/℃
α_u	5.25×10^{-5}	5.25×10^{-5}	5.25×10^{-5}	1/℃
ρ_{sT_0}	2.63	2.63	2.63	g/cm^3
ρ_{wT_0}	0.998	0.998	0.998	g/cm^3
λ_w	0.6	0.6	0.6	$W/m/$℃
λ_s	2.56	2.56	2.56	$W/m/$℃
C_s	732	732	732	$J/kg/$℃
C_w	4186	4186	4186	$J/kg/$℃
k_{vT_0}	1.8×10^{-8}	2.0×10^{-8}	2.8×10^{-8}	m/s
e_k	4.68	4.68	4.68	-
C_k	2	2	2	-
σ'_{zp0}	0.0844	0.1044	0.031	kPa
e_0	7.86	7.86	7.86	-
κ_T	0.0001	0.0001	0.0001	-
λ_T	1	1	1	-
κ	0.1954	0.1945	0.1954	-
λ	1	1	1	-
ψ	0.0520	0.0478	0.0465	-
t_0	1440	1440	1440	min

940
941